AGU ADVANCING EARTH AND SPACE SCIENCES

AGU Advances

RESEARCH ARTICLE
10.1029/2025AV002278

"Young Get Older, But Old Get Younger": Warming-Induced Circulation Change Explains Contrasting Pattern of Projected Pacific Deoxygenation

Benjamin A. Taylor[1,2], Yassir A. Eddebbar[1], Yohei Takano[3,4], Lynne D. Talley[1], and Shang-Ping Xie[1]

[1]Scripps Institution of Oceanography, University of California San Diego, La Jolla, CA, USA, [2]Department of Geosciences, Princeton University, Princeton, NJ, USA, [3]British Antarctic Survey, Cambridge, UK, [4]Earth Surface System Research Center, Research Institute for Global Change, Japan Agency for Marine-Earth Science and Technology, Yokosuka, Japan

Abstract Future projections of oxygen and water mass age change in the upper Pacific Ocean show a consistent pattern: strong deoxygenation and increased age in the well-ventilated subtropical gyres, contrasted by weak deoxygenation and younger age in the poorly ventilated tropical oxygen minimum zones. We investigate the underlying dynamics of this pattern by forcing an intermediate-complexity ocean circulation and biogeochemistry model with globally uniform and regionally-distinct idealized warming experiments. We find that this meridional contrast in oxygen and age change arises from a slowdown of vertical velocities driven by a combination of Pacific basin and remote Southern Ocean heat forcing. Warming and stratifying the upper Pacific basin compresses the subtropical gyre circulation into a shallower, flatter layer, thereby reducing ventilation along the base of the North Pacific ventilated thermocline. Warming in the mid-latitude Southern Ocean reduces downwelling locally, but remotely reduces upwelling of old, low-oxygen water in the Tropical and North Pacific via a Kelvin wave-mediated adjustment of the circulation. The combination of these two effects drives the "young get older, but old get younger" response of the Pacific thermocline. Continued monitoring of upper ocean oxygen through the Biogeochemical-Argo float program and improved model representation of mid- and high-latitude ventilation processes are critical to inform how marine ecosystems will adapt to a warmer and more stratified ocean.

Plain Language Summary Deoxygenation, the loss of dissolved oxygen (O_2) in the ocean as the climate warms, poses a serious threat to marine life. Climate models project geographically uneven deoxygenation in the Pacific basin, with the subtropical North Pacific losing O_2 substantially while the tropical Pacific experiences little O_2 loss. This contrast reflects projected changes in the average time since seawater was last in contact with the atmosphere (water-mass age), with "older" age implying more O_2 consumption (lower O_2). In the subtropical North Pacific, sinking of surface water into the thermocline (200–1,000 m depth) maintains a "young" age, but age deep within this layer increases under warming; the more isolated Tropical Pacific thermocline is "old" at present, but becomes "younger" under warming. We use a simplified ocean model to show that this geographic contrast can be explained by the adjustment of ocean currents to a warmer surface ocean and stronger stratification. Vertical currents in the ocean interior slow down as stratification increases, weakening both the downward transport of O_2-rich waters into the subtropical thermocline and the upwelling of O_2-depleted waters into the tropical Pacific. Clarifying this physical explanation informs our confidence in the climate projections and how we compare them to observed deoxygenation.

Peer Review The peer review history for this article is available as a PDF in the Supporting Information.

Key Points:

- Strong warming drives age increase and O_2 loss in the subtropical North Pacific but age decrease and weak O_2 change in the tropical Pacific
- Increased stratification in the Pacific basin shoals subtropical ventilation pathways, reducing oxygen transport to deeper layers
- Reduced subduction in the Southern Ocean dynamically weakens the upwelling of old, low-O_2 waters into the tropical thermocline

Supporting Information:

Supporting Information may be found in the online version of this article.

Correspondence to:

B. A. Taylor,
bataylor@princeton.edu

Citation:

Taylor, B. A., Eddebbar, Y. A., Takano, Y., Talley, L. D., & Xie, S.-P. (2026). "Young get older, but old get younger": Warming-induced circulation change explains contrasting pattern of projected Pacific deoxygenation. *AGU Advances*, *7*, e2025AV002278. https://doi.org/10.1029/2025AV002278

Received 2 JAN 2026
Accepted 25 JUN 2026

Author Contributions:

Conceptualization: Benjamin A. Taylor, Yassir A. Eddebbar, Lynne D. Talley, Shang-Ping Xie
Data curation: Yohei Takano
Formal analysis: Benjamin A. Taylor
Funding acquisition: Lynne D. Talley
Investigation: Benjamin A. Taylor
Methodology: Benjamin A. Taylor, Yassir A. Eddebbar, Yohei Takano
Project administration: Lynne D. Talley

1. Introduction

Dissolved oxygen (O_2) is vital to marine life and sensitive to ocean circulation change. In the interior ocean, O_2 is consumed through respiration and replenished by physical transport processes from the oxygenated surface ocean (Sverdrup, 1938; Wyrtki, 1962). Rapid ventilation, as in the subtropical North Pacific, sustains marine aerobic organisms' habitats and thus plays a critical role in shaping ocean biogeography (Deutsch et al., 2020). On the other hand, slower ventilation combined with intense O_2 demand in the eastern Tropical Pacific result in the world's most expansive oxygen minimum zones (OMZ's, Karstensen et al., 2008), where unique microbial communities play a critical role in oceanic nitrogen cycling (Lam et al., 2009). Global warming is expected to cause both broad ocean deoxygenation due to reduced O_2 solubility (Keeling et al., 2010) and a distinct spatial pattern of O_2 change in the thermocline by modulating ventilation of O_2 at depth (J. J. Busecke et al., 2022;

Resources: Yassir A. Eddebbar, Yohei Takano
Software: Benjamin A. Taylor, Yohei Takano
Supervision: Yassir A. Eddebbar, Lynne D. Talley, Shang-Ping Xie
Validation: Benjamin A. Taylor, Yohei Takano
Visualization: Benjamin A. Taylor
Writing – original draft: Benjamin A. Taylor
Writing – review & editing: Benjamin A. Taylor, Yassir A. Eddebbar, Yohei Takano, Lynne D. Talley, Shang-Ping Xie

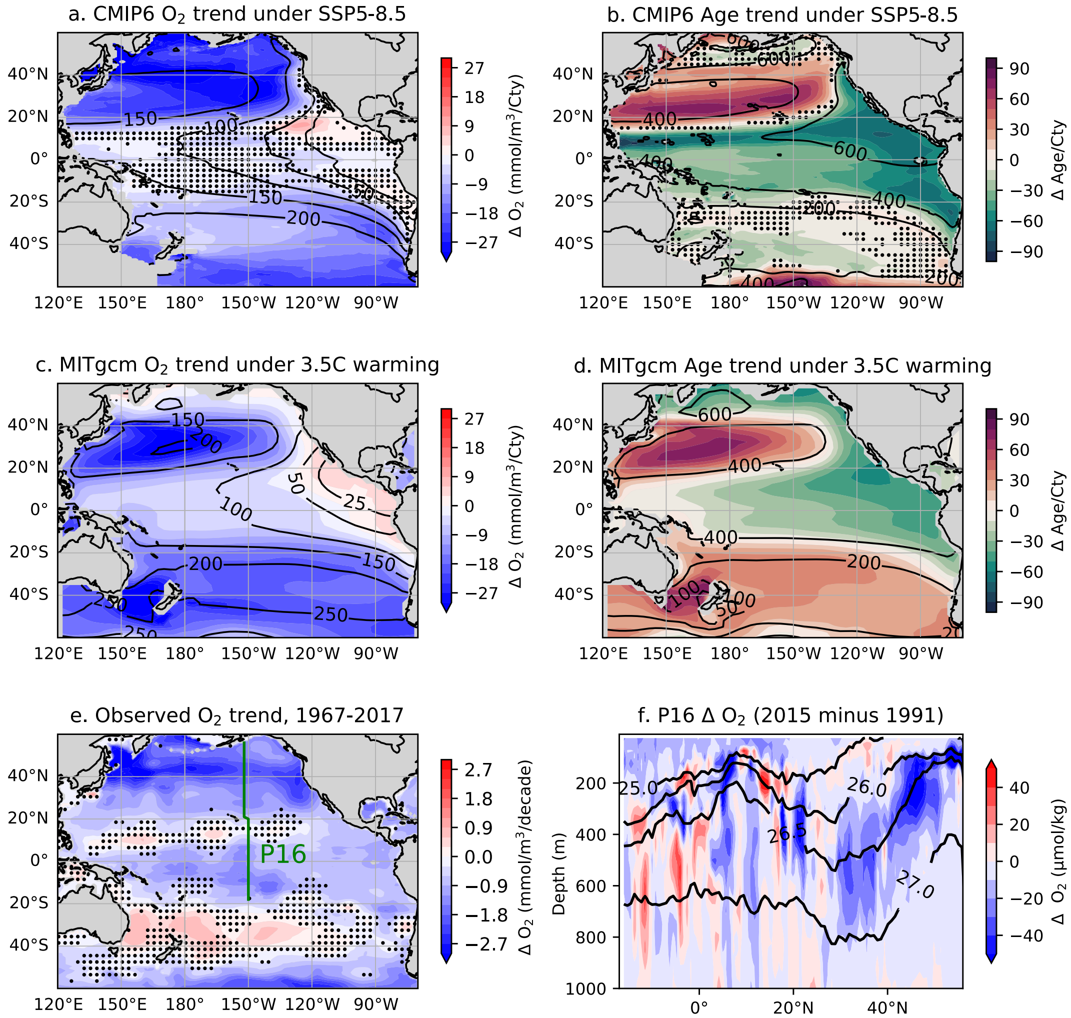

Figure 1. Trends in O_2 and age in Coupled Model Intercomparison Project 6 (CMIP6) and Massachusetts Institute of Technology General Circulation Model (MITgcm) models, averaged from 200 to 1,000 m. (a, b) CMIP6 median trends over the 21st century in the high-forcing Shared Societal Pathway 5–8.5 scenario for (a) O_2 and (b) ideal age. Stippling shows where models disagree on sign of trend (agreement of fewer than 10 of 14 models for O_2, 7 of 10 for ideal age). (c, d) Trends over the MITgcm 100-year Gradual-3.5°C spatially uniform warming run for (c) O_2 and (d) ideal age. Contours show the mean values in the respective control runs. (e) O_2 linear trend computed over the 200–1,000 m depth range using three gridded products synthesizing shipboard and Biogeochemical-Argo measurements of O_2 (see Methods; Ito, 2022; Roach & Bindoff, 2023; Ito et al., 2024); stippling shows where the sign of product trends disagree. (f) O_2 change along the P16 repeat hydrography line (150°W, plotted in green in panel (e)) between 1991 and 2015, extending Mecking et al. (2008).

Takano et al., 2018). The timescale of ventilation in ocean models is often assessed by an ideal age tracer, which represents how long a water parcel has been out of contact with atmosphere (e.g., Zhang et al., 2024). In the Pacific basin, climate models project that the well-ventilated subtropical thermocline will increase in age (corresponding to weaker O_2 ventilation), whereas the poorly ventilated tropical region becomes younger (Figures 1b and 1d); we term this phenomenon the "young get older, but the old get younger" response of the Pacific thermocline to warming. Here we present a unified explanation for this striking contrast.

The present distributions and future change in O_2 and ideal age in the Pacific basin follow the dynamical boundaries of the ventilated thermocline (Figure 1). The subtropical gyres (~150 mmol/m^3 O_2 contours in Figures 1a and 1b) advect waters subducted along their poleward edges throughout the subtropical thermocline (Luyten et al., 1983; Portela et al., 2020), keeping it relatively young and rich in O_2 (Figures 1a–1d). Coupled Model Intercomparison Project 6 (CMIP6) models under strong radiative forcing consistently project lower O_2 and older age within the subtropical gyres, especially in the North Pacific where the gyre overlies poorly ventilated deep waters (Figures 1a and 1b). Equatorward and eastward of the gyre, strong potential vorticity fronts (Talley, 1988) separate recently subducted waters from the eastern tropical Pacific thermocline ($O_2 < \sim 100$ mmol/m^3). This region is instead ventilated by several less direct pathways, including lateral advection via the equatorial current system, eddy stirring, turbulent mixing, and upwelling of intermediate waters (Bettencourt et al., 2015; Eddebbar et al., 2024; Llanillo et al., 2018; Margolskee et al., 2019). While water mass age consistently decreases in CMIP6 projections of the eastern tropical thermocline, O_2 shows a mixed response across models. This is because the warming-induced decrease in O_2 solubility roughly balances the decrease in O_2 utilization associated with decreasing age in this region (J. J. Busecke et al., 2022; Cabré et al., 2015; Takano et al., 2018). Shipboard measurements over recent decades suggest that the North Pacific thermocline has experienced substantial deoxygenation, concentrated along the densest seasonally outcropping isopycnals ($\sigma_0 = 26.5{-}26.7$), while tropical waters have also lost O_2 (Figures 1e and 1f, Emerson et al., 2004; Mecking et al., 2008). Observed deoxygenation in the North Pacific during the 20th century somewhat resembles the spatial pattern of 21st-century projections (Figures 1a and 2c), but a direct comparison is inappropriate because the observed trend is strongly influenced by internal variability, particularly the Pacific Decadal Oscillation (Duteil et al., 2018; Ito et al., 2019; Poupon et al., 2023), whereas 21st-century projections highlight the externally forced response (Long et al., 2016). Ito et al. (2026) show that this observed deoxygenation exceeds historical simulations of O_2 change in the North and tropical Pacific, but note major uncertainties in the observational reconstructions and weak agreement between CMIP6 models in the historical era (e.g., Takano et al., 2023); thus, we focus our attention on understanding the long-term forced response.

The similar large-scale structure of projected trends in ideal age and O_2, particularly its non-thermal component (approximated by negative Apparent Oxygen Utilization, $(-1) * \mathrm{AOU} = O_2 - O_{2,sat}$), suggests ventilation change as the underlying driver of these deoxygenation patterns (Bopp et al., 2017; Couespel et al., 2026). In principle, O_2 utilization depends on both the timescale of physical ventilation (age) and the O_2 utilization rate (OUR, the biological respiration rate) (Feely et al., 2004; Jenkins, 1982; Sulpis et al., 2023), though biological changes may play some independent role (Cabré et al., 2015). However, tropical OUR variability tends to amplify physically-driven O_2 variability: increased tropical upwelling simultaneously increases thermocline age and net primary productivity, both corresponding to thermocline O_2 loss (Deutsch et al., 2011; Ito et al., 2019). Variability and trends in Pacific thermocline ventilation are frequently attributed to changes in wind stress (e.g., Deutsch et al., 2014; Duteil et al., 2014). However, idealized model experiments (Takano et al., 2018) suggest that surface warming is the primary forcing causing the "young get older, but old get younger" response on centennial timescales, while wind stress changes induce weaker and unrelated patterns of O_2 and age change. Ito et al. (2022) further showed that the contrast between subtropical and tropical deoxygenation under long-term warming is strongest with weak mixing parameters, suggesting that this spatial contrast is sharpened by changes in large-scale advection and damped by mixing between the subtropics and tropics (e.g., Couespel et al., 2019; Lévy et al., 2022).

Several circulation changes have been suggested to explain some aspect of this contrasting tropical-subtropical thermocline O_2 and age response to future warming. Gnanadesikan et al. (2007) first proposed that the rejuvenation of tropical Pacific interior waters results from reduced upwelling of "old deep" waters below the tropical thermocline, which they link to a weakening of the global overturning circulation and thus to changes in high-latitude forcing. Gnanadesikan et al. (2012) extended the reduced-upwelling argument to tropical O_2, but also noted a role for local ventilation changes along the eastern boundary. The dynamics linking North Atlantic buoyancy forcing with the Tropical Pacific thermocline depth have been recently elucidated by Sun et al. (2022), again suggesting a potential role for remote forcing in driving the tropical response. In contrast, thermocline O_2 variability in the subtropical North Pacific has been attributed to surface forcing of the upstream outcrop regions (Kwon et al., 2016; Mecking & Drushka, 2024), with little consideration of forcing outside the Pacific basin. Increased stratification under warming shoals mixed layers and thus somewhat limits subduction (e.g., Liu & Wang, 2014); this has been hypothesized to thin the ventilated layers (Oschlies et al., 2018) or to slow the subtropical cell circulation (J. J. Busecke et al., 2022). Both hypotheses are consistent with subtropical deoxygenation, but lack an explanation for the contrasting tropical response or the underlying dynamics. However, recent modeling experiments (Peng et al., 2022; Wang et al., 2015) show that warming-driven stratification also shoals the vertical structure of the subtropical geostrophic circulation, leading to surface acceleration and weaker flow at depth. These circulation changes effectively flatten the isopycnals of the lower thermocline, acting to limit warming at depth precisely within the subtropical gyres (Newsom et al., 2022; Taylor et al., 2025; Wang et al., 2015). The analogous effect on O_2 and age has not yet been explored.

Here, we use idealized model simulations to isolate and illustrate the warming-induced circulation changes that drive the "young get older, but old get younger" pattern in the Pacific thermocline under projected climate change. We choose a relatively simple ocean model with biogeochemistry that reproduces this contrasting pattern of deoxygenation under a uniform warming perturbation with climatological winds (Figures 1a–1d, Section 2). Next, we perturb the sea surface temperature (SST) in different regions to assess the relative roles of local increase in stratification (Pacific basin warming) versus dynamical adjustments to remote forcing (Southern Ocean or North Atlantic warming). We present age and O_2 anomalies driven by each SST perturbation in Section 3, then connect these anomalies to the underlying circulation change using age and O_2 budget analysis in Section 4. We show that Pacific warming drives age increase and O_2 loss at depth in the subtropical gyre, which we tie to the stratification-driven shoaling of circulation. On the other hand, tropical age decrease is linked to reduced upwelling of old waters, forced remotely via Kelvin waves by weakened downwelling in high latitude water mass formation regions such as the mid-latitude Southern Ocean. Finally, we summarize our results and discuss the implications of our findings for understanding future O_2 change in Section 5.

2. Model Experiments and Data Sets

2.1. Observations and CMIP6 Models

To show the mean observed distribution of O_2 in the modern ocean, we use the World Ocean Atlas 2023 O_2 product (H. Garcia et al., 2024) (contours in Figures 2a and 2b). To estimate change over the past decades, we average three gridded observations-based products of oxygen change that use distinct mapping techniques: Roach and Bindoff (2023) is based on variational analysis, Ito (2022) uses optimal interpolation (we use a version extended through 2017), and Ito et al. (2024) uses machine learning algorithms. Ito et al. (2026) provides a detailed comparative analysis of these data sets and their uncertainties. We also show the changes in O_2 along repeat hydrography transects P16 and P02 at 150°W and 30°N, respectively (Figure 1f and Figure S1 in Supporting Information S1). We use the 14 CMIP6 models with O_2 output (10 of which also have ideal age), namely ACCESS-ESM1-5, CNRM-ESM2-1 (no age), CanESM5, CanESM5-CanOE, GFDL-CM4, GFDL-ESM4, IPSL-CM6A-LR, MIROC-ES2L, MPI-ESM1-2-HR (no age), MPI-ESM1-2-LR, MRI-ESM2-0 (no age), NorESM2-LM, NorESM2-MM, and UKESM1-0-LL (no age) (Table S1 in Supporting Information S1). These data sets were consolidated and regridded by J. J. Busecke et al. (2022).

2.2. Ocean Model Setup and Validation

Our primary tool is an intermediate complexity version of the Massachusetts Institute of Technology General Circulation Model (MITgcm) (Marshall, Adcroft, et al., 1997; Marshall, Hill, et al., 1997) coupled to a simple biogeochemistry model (Dutkiewicz et al., 2005; Parekh et al., 2005). The horizontal grid resolution is 2.8°, and there are 23 nonuniform vertical levels. There is no Arctic Ocean and minimal representation of marginal seas (e.g., no Mediterranean Sea). In our model, biological production is limited by light availability and phosphate (PO_4) and iron (Fe) concentrations. The resulting organic matter is partitioned between dissolved and sinking forms at a constant rate, and the sinking form is remineralized according to a Martin curve. We spin up the model for 4,000 years using climatological wind stress, freshwater flux, and heat flux (Jiang et al., 1999; Trenberth et al., 1990). To maintain surface temperature-salinity properties close to observations, we also applied Newtonian relaxation to the SST and salinity toward monthly climatology (Levitus et al., 1994) with timescales of 60 and 90 days, respectively. An idealized age tracer is initialized at small values at the beginning of the spin-up and allowed to equilibrate. While ideal age is still trending upward in the abyssal Pacific at the end of the spin-up, age in the North Pacific above 1,000 m depth has stabilized. A similar configuration of MITgcm has been used in idealized experiments to study the sensitivity of ocean deoxygenation to climate forcings and mixing parameters (Ito et al., 2022; Takano et al., 2018).

Physical parameters are chosen to minimize the mismatch from World Ocean Atlas O_2 concentrations (H. E. Garcia et al., 2019). We adjusted two mixing parameters: vertical diffusivity in the upper 2,000 m from the vertical mixing scheme of Bryan and Lewis (1979) and the Redi coefficient for along-isopycnal diffusivity of tracer concentration (Redi, 1982). The Gent-McWilliams isopycnal thickness diffusivity is set to the canonical value of 1,000 m^2/s (Gent & Mcwilliams, 1990). We also optimized adjustments of the high-latitude surface salinity restoring value away from climatological salinity in an effort to moderate the strength of ventilation in high-latitude regions. Beginning with the parameter values suggested by the parameter sweep of Ito et al. (2022),

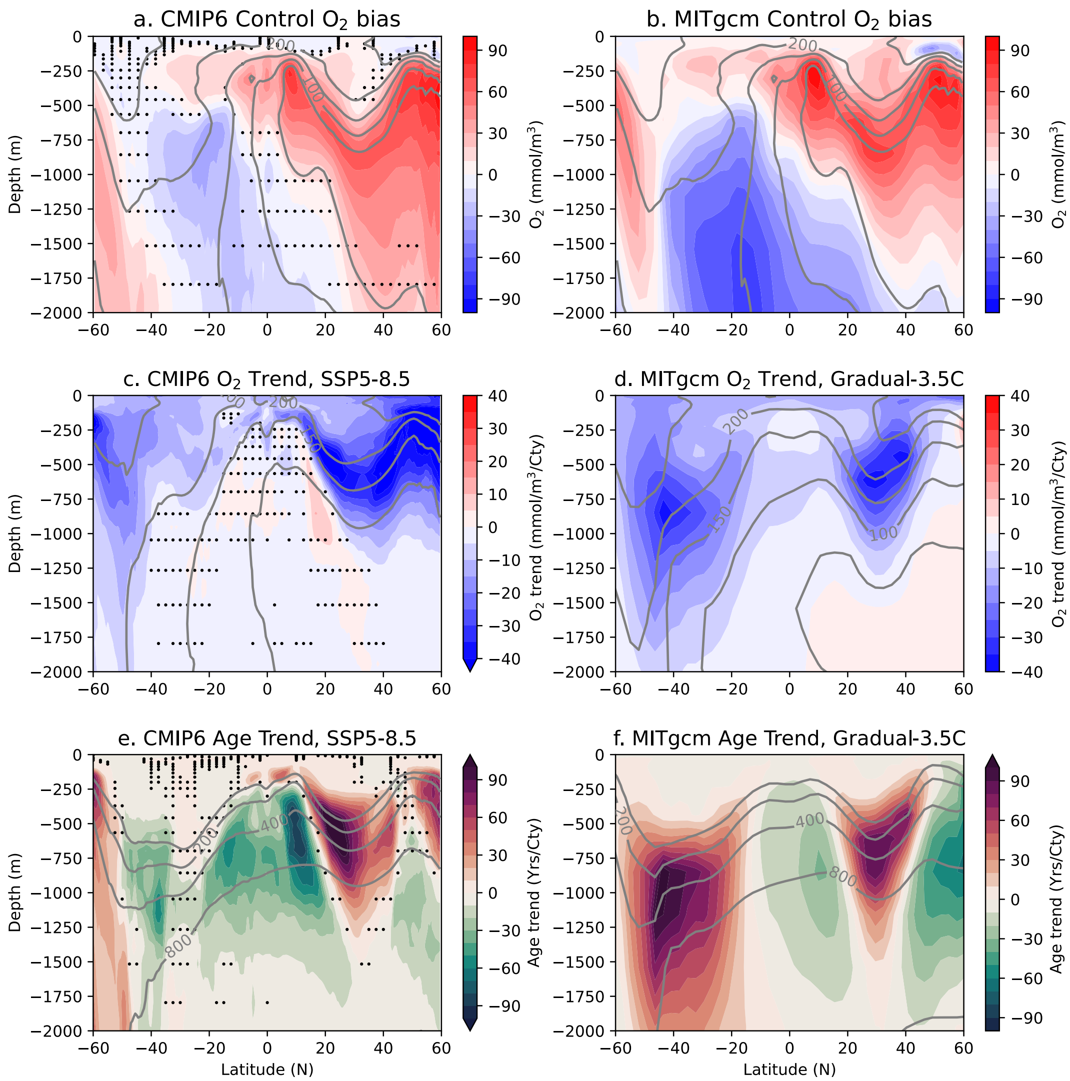

Figure 2. Oxygen and age from the Coupled Model Intercomparison Project 6 (CMIP6) multi-model mean and the Massachusetts Institute of Technology General Circulation Model (MITgcm) model in the central Pacific. All panels show the central Pacific zonal mean (150°E–150°W). (a, b) Bias of the CMIP6 ensemble mean pre-industrial O_2 (a) and MITgcm control run (b) with respect to WOA23; contours are WOA23 O_2 levels. (c–f) CMIP6 SSP5-8.5 ensemble median linear trend from 2000 to 2100 versus a gradual 3.5°C sea surface temperature change trend over 100 years in the MITgcm model. Color shading shows the change, whereas contours show the mean value. (c, d) O_2 change; (e, f) ideal age change. Stippling shows where CMIP6 models do not agree on sign: agreement of fewer than 10 of 14 models for O_2 (a, c), 7 of 10 for ideal age (e).

we optimized the representation of AOU (ventilation rate) compared to observations by applying a Green's function method to a set of parameter perturbations (e.g., Kuhn et al., 2025). Ultimately, we selected values of: upper 2,000 m ocean vertical mixing $= 1.5e - 5\,\mathrm{m}^2/\mathrm{s}$, Redi coefficient $= 1500\,\mathrm{m}^2/\mathrm{s}$, Southern Ocean salinity adjusted upward by 0.2 psu south of 60°S (similar to Ito et al., 2022; Takano et al., 2018), and North Pacific salinity reduced by 1 psu north of 48°N with a stepped reduction to the south.

The MITgcm control run captures the observed large-scale structure of the CMIP6 mean pre-industrial O_2 well (see Figures 2a and 2b and grey contours in Figures 2c and 2d). A large low O_2 zone ($O_2 < 60$ mmol/m^3) occupies most of the North and tropical Pacific, while the southern hemisphere of the Pacific basin (south of 40°S) is generally well oxygenated, in line with the WOA23 climatology and CMIP6 structures. There are notable O_2 biases in the MITgcm spun-up state: excess oxygenation of the North Pacific and the shallow tropical OMZs, reflecting a model that might be too diffusive in these regions, and deficient oxygenation of the Southern Hemisphere intermediate waters. These biases are overall similar to the mean CMIP6 model bias (Figures 2a and

Table 1
Description of the Massachusetts Institute of Technology General Circulation Model Experiments; Regions Are Mapped in Figure 3

Simulation	ΔSST distribution	ΔSST time pattern
Control	None	None
Gradual-3.5C	Globally uniform	Linear trend
Global-4C	Globally uniform	Immediate Step
Pacific-4C	Region 1	Immediate Step
Southern-4C	Region 2	Immediate Step
NAtlantic-4C	Region 3	Immediate Step
LowLat-4C	Region 4	Immediate Step

Note. All simulations are run for 100 years.

2b) and reflect longstanding issues in modeling the oceanic O_2 cycle, such as poor representation of eddy mixing, remineralization rates, intermediate water ventilation, and the equatorial current system (Cabré et al., 2015; Duteil et al., 2021; Ito et al., 2026; Kwiatkowski et al., 2020).

2.3. MITgcm Experiments

We conduct idealized perturbation experiments in which all or only one region of the ocean surface is restored to elevated SST's, each considered as a difference from a 100-year control run. In all experiments, the applied wind stress is held at climatological values and sea surface salinity is restored to climatology (though salinity restoring does generate some anomalous freshwater fluxes in response to changing ocean circulation). We include a gradual uniform warming experiment of comparable magnitude to warming under SSP5-8.5, the CMIP6 scenario with the strongest radiative forcing, to demonstrate how spatially uniform warming can reproduce substantial components of the projected O_2 change.

We next perform the five SST 4°C step increase experiments shown in Table 1 (Figure 3), which simulate how heat addition in distinct regions impacts Pacific O_2 and age change. The sudden SST increase experiments separate the timescales of the various responses to warming (as in Taylor et al., 2025) and allow the thermocline to equilibrate to the new boundary condition. The results are qualitatively similar when SST is instead increased gradually; compare the transient global warming Gradual-3.5C results (Figures 1c, 1d, 2d, and 2f) with sudden Global-4C (Figures 4a, 4b, 5a, and 5d). This similarity demonstrates the importance of sustained circulation changes as opposed to transient effects such as the more rapid response of the subtropics to surface perturbations. Pacific-4C investigates the effects of increased stratification due to heating of the Pacific basin, described herein as "local" effects. Southern-4C and NAtlantic-4C consider heat addition at higher latitudes outside the Pacific basin, which evaluates the "remote" impacts of changes in mode, intermediate and deep water formation and adjustments in the global overturning circulation. The transition between the Pacific-4C and Southern-4C forcing regions is tapered over 39–48°S; Southern-4C forcing thus impacts the denser classes of mode and intermediate waters that ventilate the South Pacific thermocline. LowLat-4C covers the remaining ocean (i.e., Indian Ocean and Tropical Atlantic), which is connected to the Pacific basin via the Indonesian Throughflow (ITF).

2.4. MITgcm Age and O_2 Budgets

MITgcm allows the online computation of closed Eulerian budgets for the O_2 and age tracers, including separate zonal, meridional, and vertical components. We output each term as an annual average for a given interior grid cell:

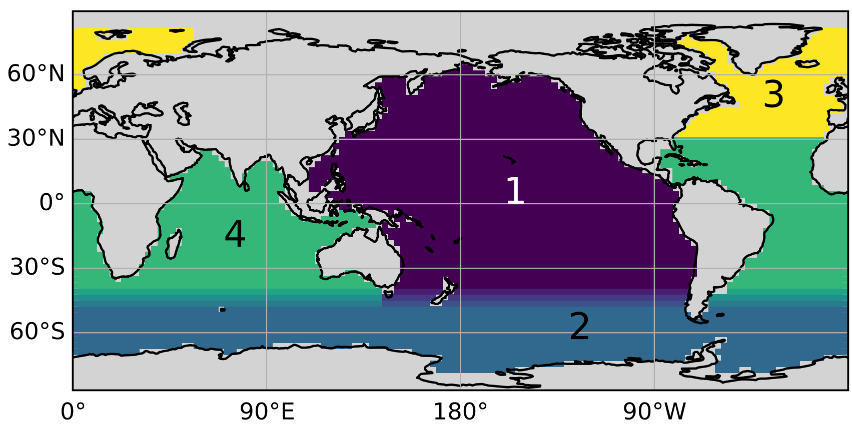

Figure 3. Map of forcing regions listed in Table 1. The fade along the northern boundary of the Southern Ocean shows the tapered forcing pattern.

$$\partial(\text{Age})/\partial t = -\nabla \cdot (\text{Age} * \vec{u}) + \nabla \cdot (\kappa \nabla \text{Age}) + 1 \tag{1}$$

$$\partial \text{O}_2/\partial t = -\nabla \cdot (\text{O}_2 * \vec{u}) + \nabla \cdot (\kappa \nabla \text{O}_2) + Bio \tag{2}$$

The age budget is unitless; in the steady state, the advection and diffusion of age must sum to -1 at every interior grid cell to compensate the positive aging tendency ($+1$). In the O_2 budget, the advection and diffusion terms balance the biological source/sink term (*Bio*), which is positive for primary productivity and negative for respiration. In the surface grid cells (not shown), age is reset to 0 and O_2 equilibrates with the prescribed atmospheric O_2 concentration via a parameterized air-sea flux. We save the total advective and diffusive fluxes across each grid cell face, then compute the divergence (using the xgcm package, Abernathey et al., 2020) to assess the net effect of advection and diffusion in each cell. To isolate the vertical and lateral components of advection, we convert the tracer fluxes into the advective form by removing the components of volume divergence:

$$ADV_z = -w(\partial C/\partial z) = -\partial_z(wC) + C\frac{\partial w}{\partial z}, \quad ADV_h = -u_h \cdot \nabla_h C = -\partial_x(uC) - \partial_y(vC) + C\left(\frac{\partial u}{\partial x} + \frac{\partial v}{\partial y}\right), \tag{3}$$

where concentration C is age or O_2. This is permissible in an incompressible fluid, because

$$-\nabla \cdot (\vec{u}C) = -u\frac{\partial C}{\partial x} - v\frac{\partial C}{\partial y} - w\frac{\partial C}{\partial z} - C\left(\frac{\partial u}{\partial x} + \frac{\partial v}{\partial y} + \frac{\partial w}{\partial z}\right) = -w\frac{\partial C}{\partial z} - u_h \cdot \nabla_h C. \tag{4}$$

Throughout the text, we use "ventilation increase" to describe the physical change that reduces age and increases O_2 (or particularly, decreases AOU) in a given location.

2.5. Comparison of CMIP6 Projections and MITgcm Gradual Warming

We first compare the Pacific age and O_2 responses of coupled climate models under intense global warming with a spatially uniform warming perturbation of similar magnitude applied to the MITgcm model. Takano et al. (2018) demonstrated that a similar MITgcm model forced with uniform warming as well as projected wind stress and freshwater flux anomalies reproduces closely the O_2 changes projected by CMIP5 models under RCP8.5. In this work, we compare the linear trend over the 21st century under SSP5-8.5 in the CMIP6 models (Figures 1a, 1b, 2c, and 2e) with the linear trend over 100 years of the Gradual-3.5C experiment (Figures 1c, 1d, 2d, and 2f), in which only SST is perturbed.

First, we note that the contrasting pattern of ventilation change in the CMIP6 ensemble median, of decreased ventilation in the North Pacific subtropical gyre and increased ventilation in the tropical ocean, is well reproduced in the MITgcm transient warming run (depth-averaged in Figures 1a–1d, zonally-averaged in Figures 2c–2f). In both the CMIP6 median and MITgcm, the North Pacific deoxygenation and age increase is confined to the well-ventilated upper ocean, with a weak increase in ventilation in the deep, poorly oxygenated waters below (Figures 2c–2f). While there is considerable diversity in ΔO_2 patterns among CMIP6 models (Figure S2 in Supporting Information S1), every model shows stronger deoxygenation in the North Pacific subtropical gyre than the eastern tropics (as shown in J. J. Busecke et al., 2022); further, MITgcm shows weak deoxygenation rather than oxygen gain in the western tropical Pacific, consistent with the projections of the higher-skilled models identified in Ditkovsky and Resplandy (2025) (Figures S2a-S2g in Supporting Information S1). CMIP6 age changes are more spatially consistent across models than O_2 changes, with age increasing in the North Pacific gyre but decreasing in the tropical shadow zones in each model (Figures 1b and 2e, Figure S3 in Supporting Information S1). Although the Gradual-3.5C experiment is forced with only SST changes, its age trend has reasonable quantitative agreement with the CMIP6 median between 20°S and 40°N. We note that the heightened age changes along the North Pacific subtropical-tropical boundary in CMIP6 are only weakly reproduced by MITgcm Gradual-3.5C, perhaps due to MITgcm's coarse resolution or the unperturbed wind stress.

Outside of 20°S–40°N, the discrepancies in ventilation change between the CMIP6 median and MITgcm are more notable (particularly in the zonal mean view, Figures 2c–2f). CMIP6 models have a mixed age response in the extratropical South Pacific, whereas MITgcm shows a deep-reaching age change indicative of a sharp reduction in Southern Ocean mode and intermediate water ventilation. Note that the strengthening of Southern Hemisphere westerly winds in the CMIP6 experiments, which accelerates the ventilation of the South Pacific thermocline (Getzlaff et al., 2016; Hollitzer et al., 2024; Takano et al., 2018), is absent in our warming-only MITgcm experiment and likely contributes to this difference. In the subpolar North Pacific, the MITgcm Gradual-3.5C shows strong age decrease and a slight oxygenation along the northern boundary, opposite the strong upper ocean deoxygenation projected by many CMIP6 models (Figures 1a–1d and 2e–2h). However, there is substantial inter-model spread in the subpolar North Pacific (Figures S2 and S3 in Supporting Information S1), and both CMIP6 models and MITgcm struggle to accurately represent this region's strong oxycline (Figures 2a and 2b). In Section 5.1, we revisit MITgcm's relatively strong South Pacific ventilation decrease and subpolar North Pacific ventilation increase in light of our Southern Ocean warming experiment. However, our primary focus is on the large-scale contrast in ventilation change between the tropical and subtropical North Pacific, which is consistent across state-of-the-art models and robustly captured by MITgcm under a warming-only experiment.

3. Ventilation Change Driven by Regional Warming

We evaluate the local versus remote impacts of surface warming on interior age and O_2 using the 4°C SST step-increase perturbation to individual regions of the ocean (see Section 2.3), and attribute their effects in the context of the global step SST perturbation of the same magnitude (Global-4C, Figure 4). Warming over the Pacific basin leads to a dramatic increase in ideal age, concentrated in the center of the relatively young subtropical gyres (Figure 4c). Rather than spreading from the regions of subduction, age increase and O_2 loss is centered at the bottom of the subtropical bowl, between 500 and 1,000 m depth around 30°N (Figure 5b). This strong O_2 loss along the base of the ventilated thermocline is similar to CMIP6 projections (Figure 2c) and to some degree historical observations (Figure 1f, Figure S1b in Supporting Information S1). The age increase extends beyond the subtropical boundary (approximately the 400-year age contour) into regions where age decreases under Global-4C (Figures 4a and 4c). Remarkably, the zonal mean perspective reveals that the equatorial ocean experiences little age change at any depth, even after a century of very strong local forcing. While our primary focus is on the tropical and subtropical North Pacific, we note that the western South Pacific subtropical gyre shows a similar response to the North Pacific, albeit with a weaker magnitude.

In contrast, remote forcing from the Southern Ocean drives a widespread decrease in age across the tropical and North Pacific that contrasts sharply with an increase in age over most of the South Pacific (Figure 4e). Southern Ocean warming impacts the formation region of mode and intermediate waters as well as Antarctic Bottom Waters, with the potential to slow both the upper and lower Pacific limbs of the global overturning circulation. The spatial distribution of this age decrease is not uniform in the North Pacific: the tropics, eastern boundaries, and North Pacific coast—all regions of mean upwelling - show intense rejuvenation, whereas the center of the North Pacific subtropical gyre shows weaker age decrease. The mid-latitude South Pacific experiences intense aging concentrated in the 1,000–2,000 m depth range, consistent with a reduction in intermediate water formation (Figure 5c). This aging signal extends northward from the southeastern Pacific following the subtropical-tropical boundary - consistent with an advective pathway. Warming in the Indian and Atlantic basins drives a rejuvenating response in the tropical and North Pacific with a similar spatial pattern as the Southern-4C experiment but a weaker magnitude (Figures S5b and S5c in Supporting Information S1); unlike Southern-4C, these other forcings do not cause aging or deoxygenation in the subtropical South Pacific. The sum of all regional forcings largely reproduces the tropical-extratropical contrast and magnitude change in the Pacific basin in the Global-4C, with only minor differences in the western tropical Pacific and northeastern Pacific (Figure S5d in Supporting Information S1).

The imprint of regional changes in ventilation as represented by ideal age is clearly evident in the patterns of O_2 and especially (–)AOU change. Regions of greatest O_2 loss are consistently those that age the most, and regions that gain O_2 all become younger (Figures 4 and 5a–5f). An important difference between the vertical distributions of O_2 and age change (Figure 5) is the broad O_2 decrease related to reduced solubility, which is prominent in the upper 500 m of regions where a 4°C SST increase is applied (Figure 5g–5i). Changes in $-1 * \text{AOU}$, in which the impact of warming on O_2 solubility is removed, correspond almost exactly to age change (Figures 5a–5c and 5j–5l), demonstrating the central importance of circulation change to AOU change in this model. Analogous to age, this model's OMZ core, located along the coast of Central America, appears to gain or maintain O_2

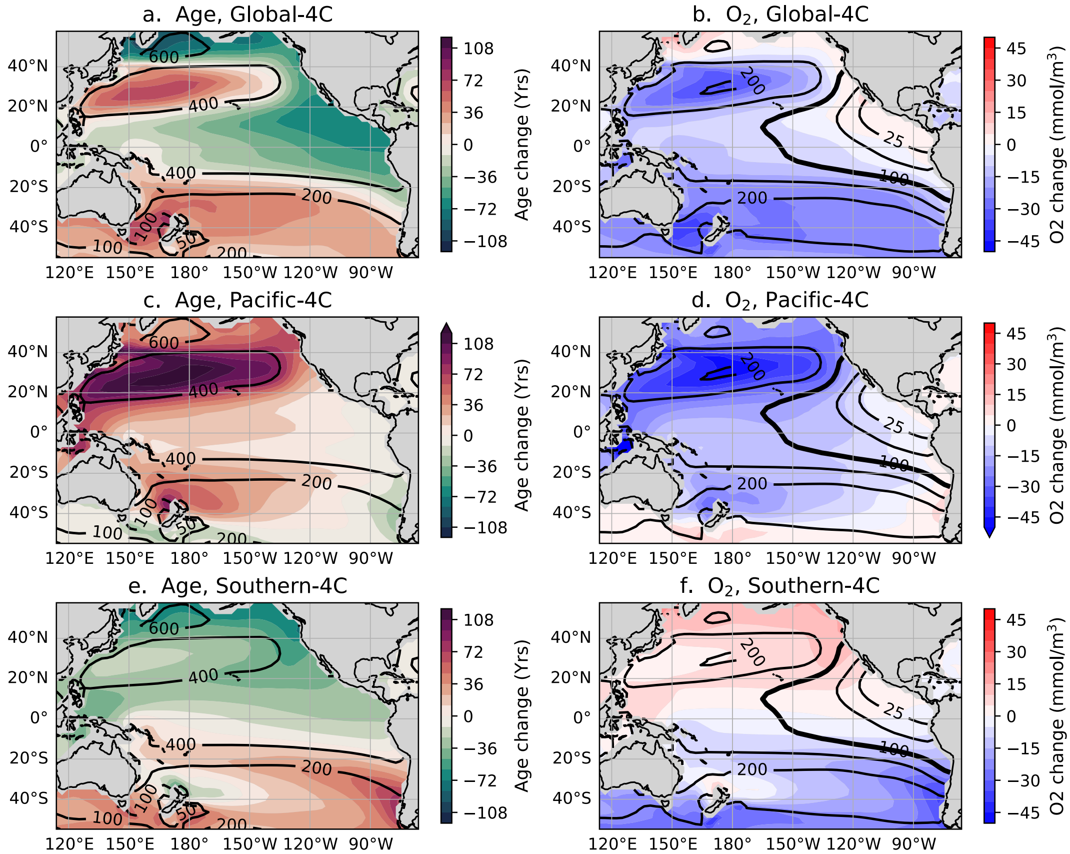

Figure 4. Ideal age and O_2 change for regional sea surface temperature forcing runs. Ideal age and O_2 anomalies relative to their control runs are averaged over 185–985 m depth for years 91–100 of each experiment. (a, b) Global-4C. (c, d) Pacific-4C. (e, f) Southern-4C. Contours show mean values from the control run; the bold contours of $O_2 < 100$ mmol/m^3 in the eastern Tropical Pacific are the OMZ boundary used in Figure 9.

concentration in each warming experiment (Figure 4), consistent with Ditkovsky and Resplandy (2025). Thus, our regional experiments show that the "young get older, but old get younger" response to warming and its imprint on O_2 results from the superposition of contrasting ventilation changes driven primarily by local forcing over the Pacific basin and remote forcing from the Southern Ocean.

4. Dynamics of Regional Ventilation Changes

The impacts of regional forcings on age and O_2 illustrated in Section 3 raise several important questions. First, what causes the strong decrease in ventilation at the base of the subtropical gyre under global, and more notably, Pacific-4C forcing? Second, what explains the contrast between weak ventilation change in the tropics and the dramatic age increase in the subtropics under Pacific-4C forcing? Finally, why does ventilation increase in the North Pacific, especially along upwelling regions, under Southern-4C forcing? We analyze both the O_2 and age budgets to identify the leading processes driving these changes, and interpret our results in the context of the dynamical adjustment of the large-scale circulation to regional warming.

4.1. Why Does Pacific Basin Warming Reduce Subtropical Ventilation at Depth?

4.1.1. Diagnosis of Subtropical Shoaling From Model Output

We attribute the strong age increase and O_2 loss centered at 500–800 m within the North Pacific subtropical gyre under Pacific-4C forcing (Figures 5b and 5e) to the shoaling of the ventilated thermocline due to warming-induced stratification (Figures 6 and 7). To illustrate this argument, we consider the structure of the processes that establish the mean distributions of age and O_2 and how these processes change when a step SST increase is

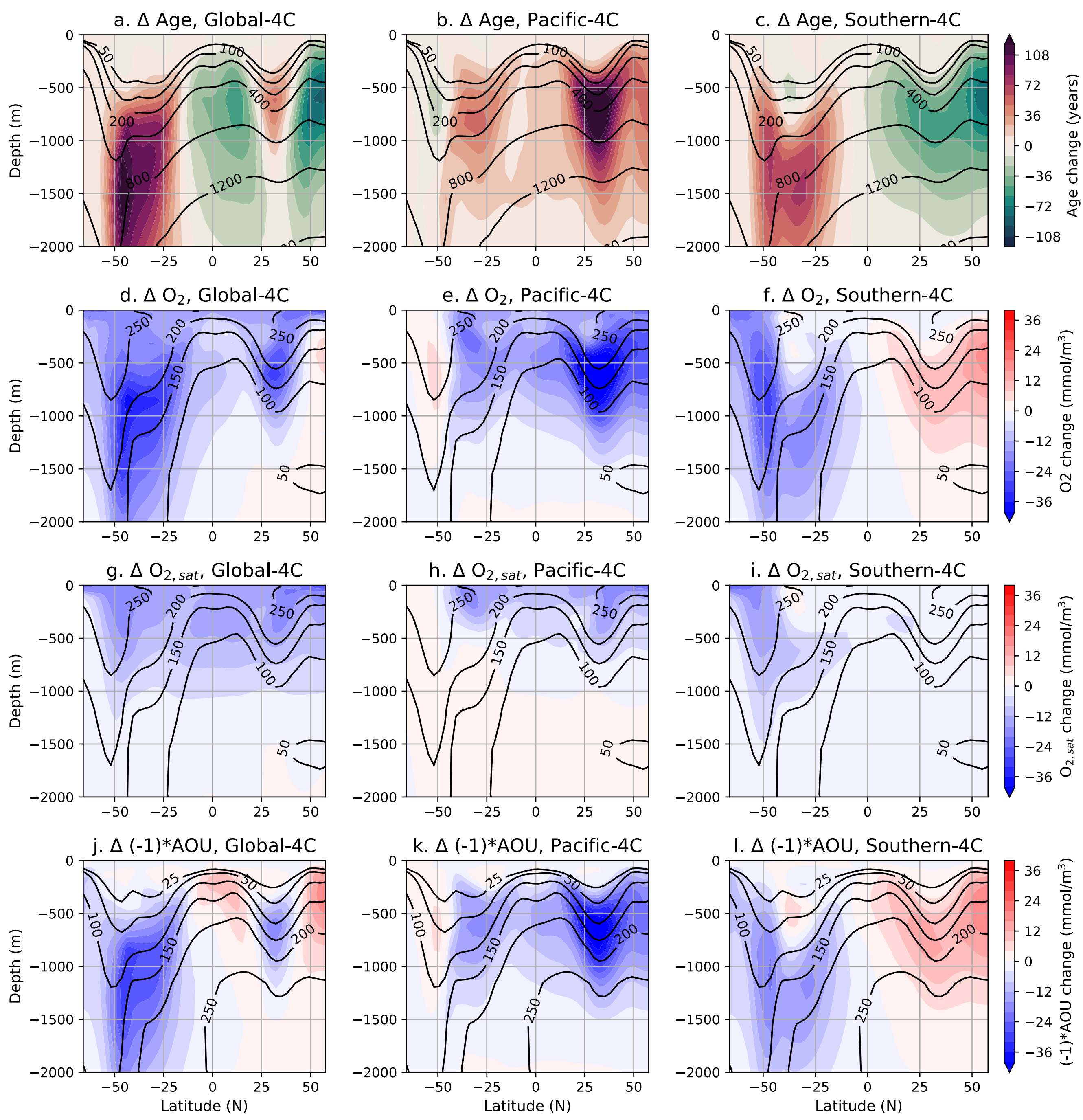

Figure 5. Zonal means of Age, O_2, $O_{2,sat}$, and $(-1) * AOU$ change in the Central Pacific under Global-4C, Pacific-4C, and Southern-4C. Zonal mean of 135°W–180°W of each tracer at years 91–100 is differenced with its control run value. Each row shows this change for one tracer: Age (a–c), O_2 (d–f), $O_{2,sat}$ (g–i), and $(-1) * AOU$ (j–l). Each column shows results from one experiment: Global-4C (a, d, g, j), Pacific-4C (b, e, h, k), and Southern-4C (c, f, i, l). Since $O_2 = O_{2,sat} - AOU$, rows (g–i) and (j–l) sum to row (d–f). Contours show tracer distribution in the control run: Age (a–c), O_2 (d–f, g–i), and (positive) AOU (j–l).

applied (Figure S6 in Supporting Information S1 and Figures 6c–6j). In steady state (Figure S6 in Supporting Information S1, also contours in Figures 6c–6j), advection—particularly vertical advection, corresponding to mean downwelling—drives strong rejuvenation (age decrease) and oxygenation within the bowl-shaped North Pacific ventilated thermocline, which is deepest around 30–35°N (Figures S6a, S6b, S6g, and S6h in Supporting Information S1). Advection is primarily balanced by diffusion for age (Figure S6c in Supporting Information S1) and both diffusion and respiration for O_2 (Figures S6d and S6f in Supporting Information S1). The spatial patterns

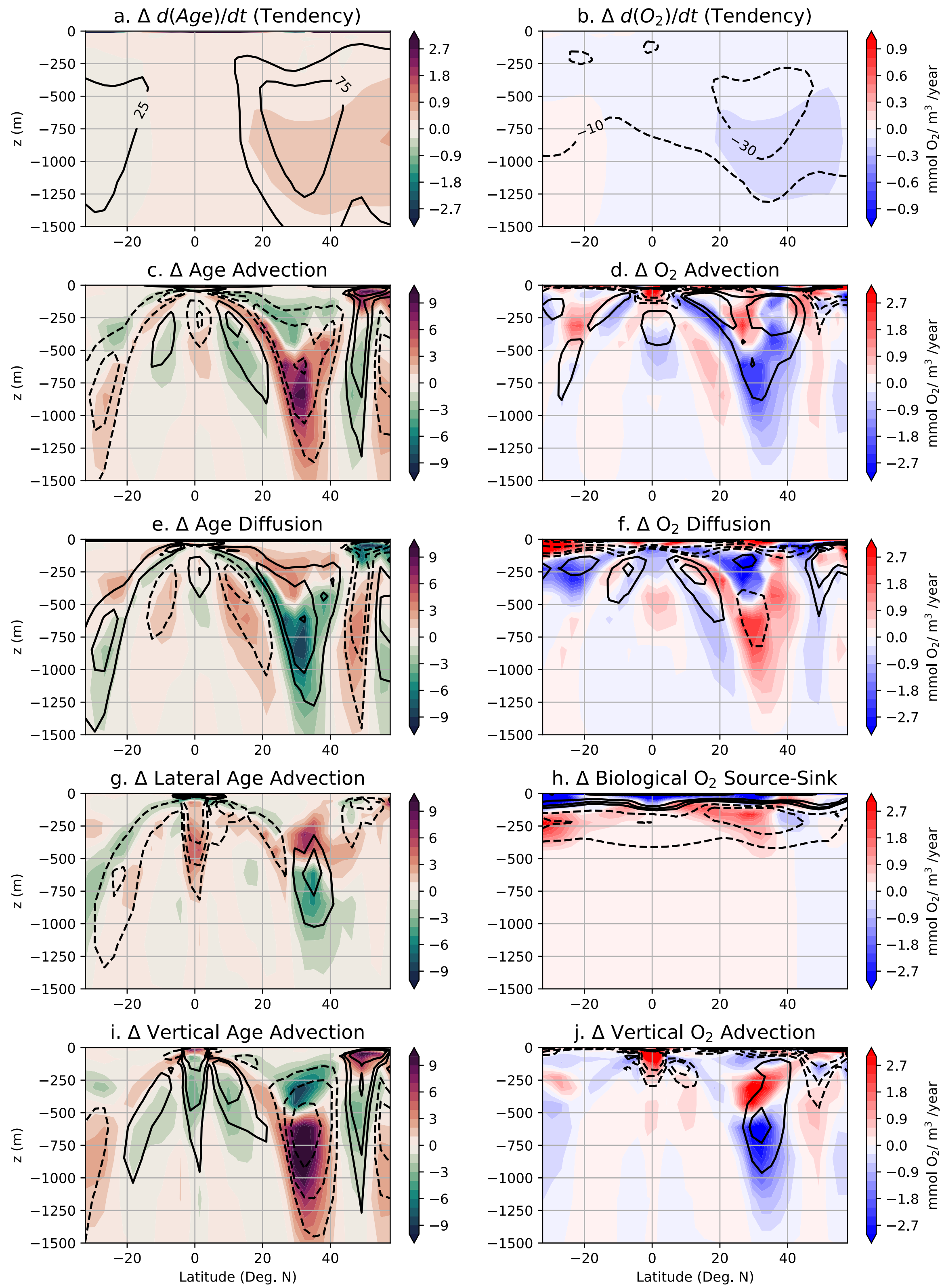
a. Δ d(Age)/dt (Tendency)
b. Δ d(O2)/dt (Tendency)
c. Δ Age Advection
d. Δ O2 Advection
e. Δ Age Diffusion
f. Δ O2 Diffusion
g. Δ Lateral Age Advection
h. Δ Biological O2 Source-Sink
i. Δ Vertical Age Advection
j. Δ Vertical O2 Advection
z (m)
Latitude (Deg. N)
mmol O2/ m3 /year

Figure 6.

of age and O_2 budget terms are generally similar (though the terms have opposite signs) because each reflects the transport processes bringing surface waters into the interior ocean. Shading in Figure 6 shows the difference between the control and the Pacific-4C run, which has nearly equilibrated to the applied SST anomaly, as shown by its small age and O_2 tendencies (Figures 6a and 6b).

In response to Pacific warming, the mean state distribution of each physical transport term shifts toward the surface. For example, age advection (Figure 6c) increases at a depth below its mean minimum (dashed contours) at 600 m depth, 30°N and decreases above this minimum, implying an upward shift of the strongest transport of young water to depth. This pattern is consistent across all terms in the North Pacific subtropics except for the biological O_2 changes (Figures 6c–6g, 6i, and 6j). The strong age increase and O_2 loss centered at 500–800 m is collocated with changes in vertical advection (Figures 6i and 6j) that reflect loss of ventilation in the deepest parts of the subtropical thermocline. The overlying region shows an increased transport of surface waters (lower age advection in Figure 6c, higher O_2 advection in Figure 6d). Together with reduced respiration (Figure 6h), this helps to reduce deoxygenation at 100–300 m depth within the subtropical gyre in this model. In the nearly equilibrated budget shown here, these changes in advection and biological processes are balanced by changes in diffusive transport (Figures 6e–6f). Our budget analysis thus reveals that shoaling of the advective transport drives the strong aging and deoxygenation in the deep subtropical thermocline simulated by our experiments and CMIP6 projections (Figures 2c and 5e).

Given the critical role of advection change in these ventilation changes, we examine the 3-D subtropical gyre velocity response to Pacific-4C SST warming and find a similar broad shoaling of its vertical structure. Both zonal and meridional velocities increase above their mean state maxima but slow down at deeper depths (Figures 7a and 7b). These lateral velocity changes reflect the pattern of advection change (Figures 6c and 6d), with more vigorous advection near the surface and weaker at depth. Vertical velocity w decreases everywhere in the interior, with weaker downwelling in the subtropics and weaker upwelling in the tropics (Figure 7c). Warming-induced changes in w are small near the surface—reflecting the control of wind stress curl on the surface vertical velocity—and largest in the subtropical thermocline. Advective transport occurs along isopycnal surfaces, so w reflects the gradual descent of waters flowing along an isopycnal layer. The reduction in w results from the flattening of isopycnal surfaces, as shown by the shoaling isopycnals in the North Pacific subtropical thermocline in Figure 7d.

4.1.2. Dynamical Explanation of Gyre Shoaling and Reduced Downwelling

The dynamical adjustment via a shoaling subtropical circulation to increased stratification due to local Pacific warming can be illustrated using a 1.5 layer model. In this simple model, there is one moving layer with depth h and vertically uniform horizontal velocity (u, v); the lower layer is stationary and denser than the upper layer by $\Delta\rho$. We make use of a reduced gravity $g' = (\Delta\rho/\rho_0)\,g$, and consider the effects of increasing g' by $\delta g'$. At the basin scale, the flow is in geostrophic balance, so we have:

$$fv = g'\frac{\partial h}{\partial x} \tag{5}$$

Taken alone, this would imply that if stratification (as represented by g') increases, either v must accelerate or $\partial h/\partial x$ must decrease (i.e., the interface slope must flatten). However, Sverdrup balance also applies. Using its vertically integrated form:

$$\beta vh = \nabla \times \boldsymbol{\tau}/\rho_0, \tag{6}$$

we substitute for v in Equation 6 and solve for h:

Figure 6. Age and O_2 budget terms for the Pacific-4C experiment averaged across 180°W–135°W. The color shading shows the budget terms averaged from years 81–100 as a difference from the control run. Age budget terms are unitless. (a, b) Tendency of each tracer; note the smaller colorbar range. Contours show the total change in age and O_2 relative to the control in the final decade (as plotted in Figures 5b and 5e). (c, d) Total advective contributions. (e, f) Diffusive contributions. Panels (g, i) lateral and vertical components of advective age transport change, which sum to panel (c). (h) Contributions of biological production and respiration of O_2. (j) Contributions of vertical transport of O_2. Contours in (c–j) show the steady state budget term contributions in the control run (also plotted in Figure S6 in Supporting Information S1); contour values are ± [5, 10, 20] for age (unitless) and ± [3, 6, 12 mmol/m^3/year] for O_2.

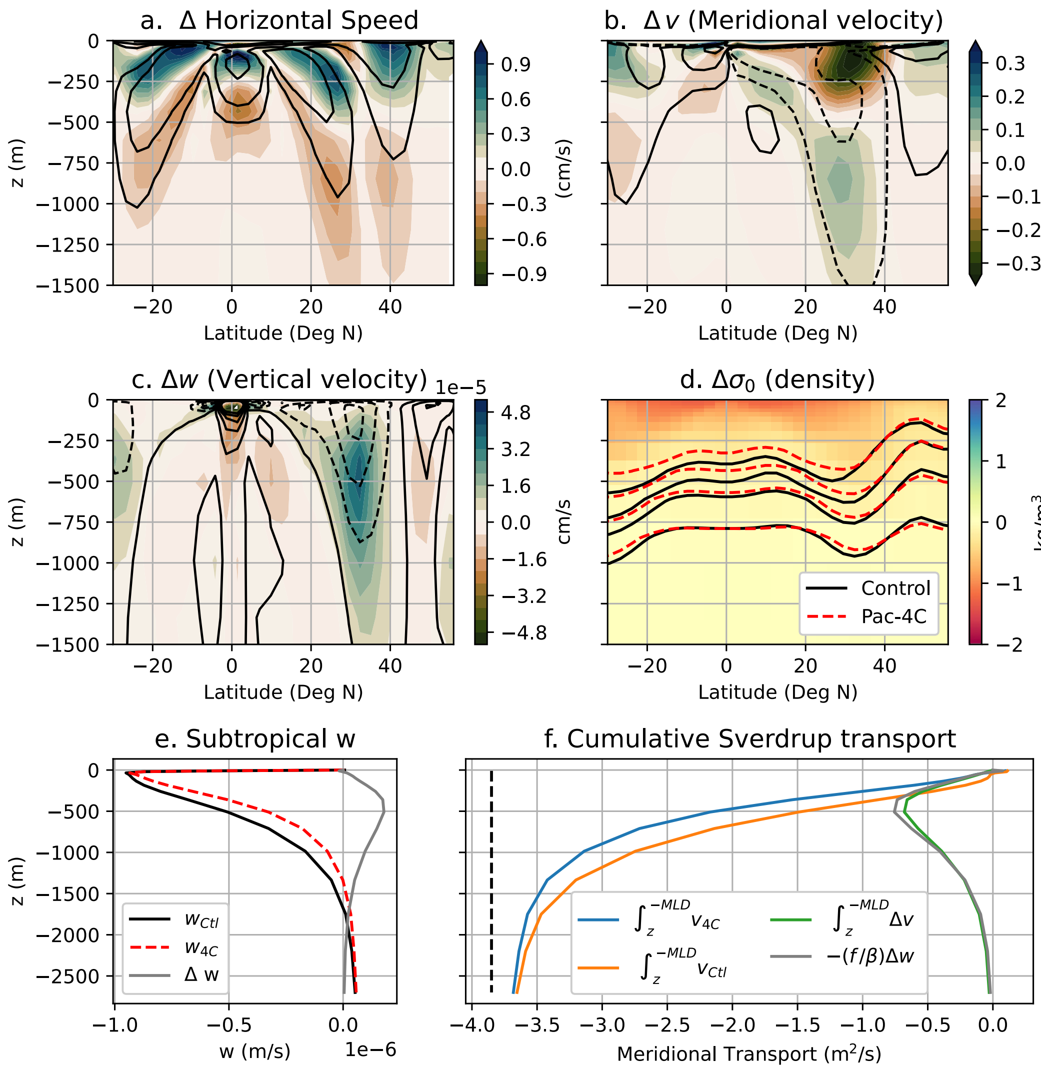

Figure 7. Physical changes in the North Pacific subtropical gyre under Pacific-4C. All quantities are shown as zonal mean across the central Pacific (180°W–135°W). (a) Horizontal speed ($\sqrt{u^2 + v^2}$) change, with contours of mean speed. (b) Meridional velocity change. (c) Vertical velocity change (positive upward). (d) Density change in color shading, lines show pairs of isopycnals from Control and Pacific-4C experiments that lie at the same depth at 40°N; paired lines do not reflect the same density, but show changes in isopycnal slope. Vertical profiles in (e) and (f) are horizontal averages over 22°N–45°N and 180°W–135°W for (e) vertical velocity, (f) total meridional transport between the surface and depth z (i.e., the cumulative sum of meridional volume transport from the surface downward). (f) also features Δw from panel (e) multiplied by a factor derived in Equation 13 and a vertical dashed line showing the Sverdrup transport predicted by the regional wind stress curl.

$$\beta\left(\frac{g'}{f}\frac{\partial h}{\partial x}\right)h = \nabla \times \boldsymbol{\tau}/\rho_0 \tag{7}$$

$$\left(\frac{\partial h}{\partial x}\right)h = \frac{f(\nabla \times \boldsymbol{\tau})}{g'\beta\rho_0} \tag{8}$$

$$g'\partial_x\left(h^2\right)/2 = \frac{f(\nabla \times \boldsymbol{\tau})}{\beta\rho_0}. \tag{9}$$

If wind stress is held constant, as it is in our experiments, the right hand side must remain constant; thus, an increase in g' requires a decreased zonal gradient of h^2. Specifically, if we make the approximation that h is small

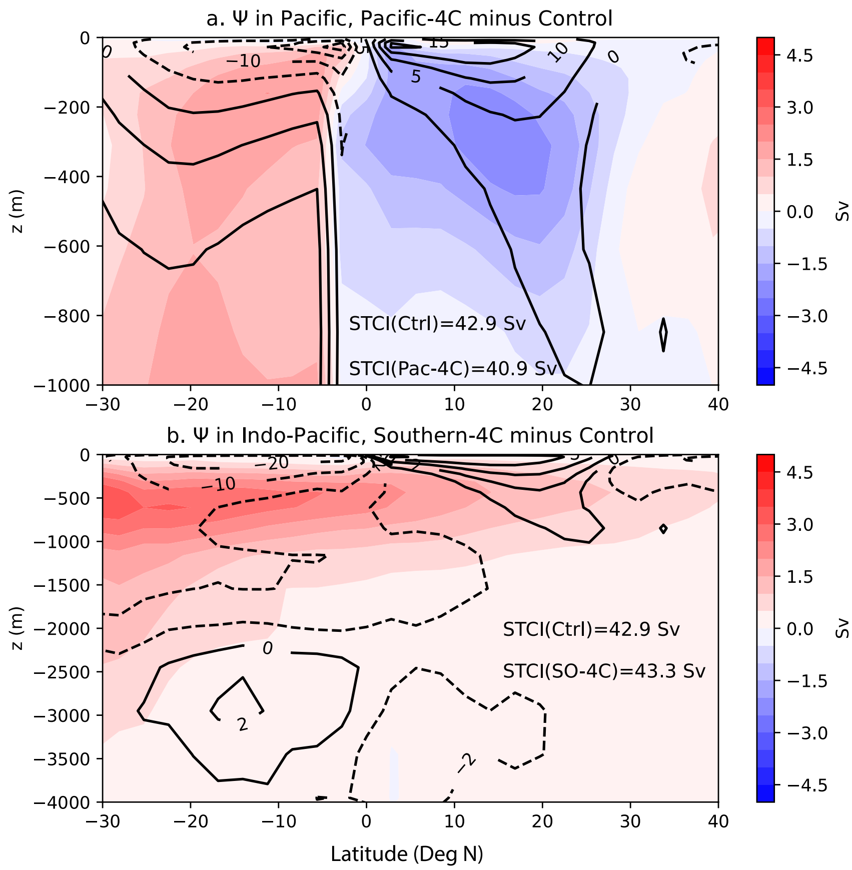

Figure 8. Overturning streamfunction change computed for Pacific-4C and Southern-4C experiments. $\Psi(y,z) = \int_x \int_z^0 v(y)\, dz'\, dx$, where the zonal integral is conducted across a specific closed basin. Subtropical Cell Index (STCI) is the difference between the maximum and minimum values of Ψ computed within the Pacific basin (assuming these extrema occur in the shallow equatorial ocean, which they do). (a) Change in the Pacific basin overturning streamfunction under Pacific-4C; contours show the control streamfunction (with 5 Sv interval). STCI values are printed for the control and Pacific-4C run. The discontinuity around 5°S (in both mean and change) is due to the Indonesian Throughflow (ITF). (b) Change in Indo-Pacific streamfunction under Southern-4C, again with control in contours (varying interval). STCI values are printed for control and Southern-4C (evaluated within the Pacific basin). Including the Indian basin eliminates the ITF discontinuity. Note that the y-axis in (a) and (b) are different to highlight different depth-dependent processes.

at the eastern boundary, we can zonally integrate from the eastern boundary to find that $g'h^2$ must also remain constant with changing g'. Then we solve for the resulting change in h, δh:

$$\frac{d}{dg'}\left(g'h^2\right) = 0 \;\Rightarrow\; 2(g'h)\,\frac{dh}{dg'} = -h^2 \;\Rightarrow\; \frac{\delta h}{h} = -\frac{1}{2}\,\frac{\delta g'}{g'}. \tag{10}$$

If we apply this idealized relationship to the MITgcm experiments, the roughly 30% increase in stratification caused by Pacific-4C warming would imply a 15% reduction in the vertical extent of the energetic circulation (h) - essentially, the subtropical ventilated thermocline depth. Indeed, our model's column-integrated Sverdrup transport is constrained to the same value in either run by the imposed wind stress, but under Pacific-4C it occurs through faster velocities within shallower depths (Figure 7f). Similarly, Figure 8a shows the subtropical overturning streamfunction weakening in magnitude at depth, indicating a shoaling of the subtropical cells; at the same time, the Subtropical Cell Index (a measure of shallow overturning strength) changes by only 2 Sv, as it is set primarily by the wind stress (McCreary & Lu, 1994). Thus, the subtropical ventilation pathways do not necessarily become more sluggish under buoyancy forcing; rather, the same volume transport reaches shallower depths, leading to a strong reduction in ventilation at depth.

The reduction in transport of oxygenated waters to depth is strongly controlled by the vertical advection change (Figures 6i and 6j) and the associated weakening of downwelling in the subtropical thermocline (Figure 7e). Whereas the near-surface vertical velocities controlling O_2 subduction into the interior (Portela et al., 2020) are set by wind-driven Ekman pumping, vertical velocity change within the subtropical thermocline is linked to the buoyancy-forced shoaling of the horizontal velocity structure. We demonstrate this using potential vorticity conservation:

$$\beta v = f \frac{\partial w}{\partial z} \tag{11}$$

Integrating from the base of the mixed layer ($z = -MLD$) to some depth z_d gives:

$$\frac{\beta}{f} \int_{z_d}^{-MLD} v dz = w(-MLD) - w(z_d) \tag{12}$$

To assess how w changes under imposed warming, we take the difference of this expression for Pacific-4C (4C) and the control run (Ctl). Importantly, $w(z = -MLD) = \nabla \times (\boldsymbol{\tau}/f\rho_0)$ is fixed by the wind stress (assuming that the Ekman layer and mixed layer depths are similar). We find that:

$$\int_{z}^{-MLD} (v_{4C} - v_{Ctl})\, dz' = -\frac{f}{\beta}[w_{4C}(z) - w_{Ctl}(z)]. \tag{13}$$

These terms are evaluated over the central subtropical North Pacific in Figure 7f, and show that the depth z at which $v_{4C}(z) = v_{Ctl}(z)$, located within the thermocline between the regions of surface acceleration and deep deceleration, is the depth of maximum change in vertical velocity ($w_{4C}(z) - w_{Ctl(z)}$). Thus, the reduced downwelling at depth, the key driver of the strong reduction of ventilation in the deep subtropical gyre, is dynamically linked to the compression of the Sverdrup transport into shallower depths.

4.2. Why Is Tropical Ventilation Relatively Insensitive to Pacific Basin Warming?

The subtropical-tropical contrast in Global-4C is driven in part by the Pacific warming: Pacific-4C not only induces a sharp decrease in ventilation in the subtropical gyre, but also yields little ventilation change in the tropics (Figures 4a–4d). While the tropics are more slowly ventilated than the subtropical gyre, 90 years is sufficient time for the strong warming and aging anomalies there to reach the eastern tropical ocean, especially at shallower depths and via along-isopycnal diffusion. Moreover, the local stratification is strongly increased throughout the tropics, which should reduce ventilation via upper ocean mixing. However, in our model, the eastern tropical thermocline decreases somewhat in age under Pacific-4C and even slightly gains O_2 along the eastern boundary Figures 4c and 4d. We show that the spread of the aging, low O_2 signal from the subtropical ocean is opposed by large circulation changes in the tropics, particularly a decrease in upwelling velocity (Figure 7c).

Vertical advection change acts to reduce age and increase O_2 in the thermocline between 20°S and 20°N (Figure 6) via a reduction of the climatological upwelling of older, low-O_2 waters. This reduction reaches its full strength within the first decade (Figures 9a and 9b), suggesting a relatively fast response of the tropical circulation to Pacific basin warming in this model—absent changes in wind stress (Luongo et al., 2025). The subtropical anomaly—higher age, lower O_2—impacts the tropics via lateral advection by the Equatorial Undercurrent (Figure 6g) as well as diffusion via isopycnal mixing along the tropical-subtropical boundary (Figures 6e and 6f). The delayed onset of diffusion and lateral advection change in the eastern tropics is associated with the timescale of transport of subtropical properties to the OMZ (Figures 9a and 9b). These changes ultimately overtake the effects of reduced tropical upwelling—after 17 years for age and less than 5 years for O_2 (Figures 9a and 9b), yielding relatively small changes in both tracers over time.

While O_2 and age both experience the same circulation changes under Pacific-4C, the tropical OMZ O_2 budget has two distinct features. Lateral advection change has a much stronger impact on O_2 than age (Figures 9a and 9b). This is likely because surface O_2 concentrations are sharply reduced by warming via decreased surface

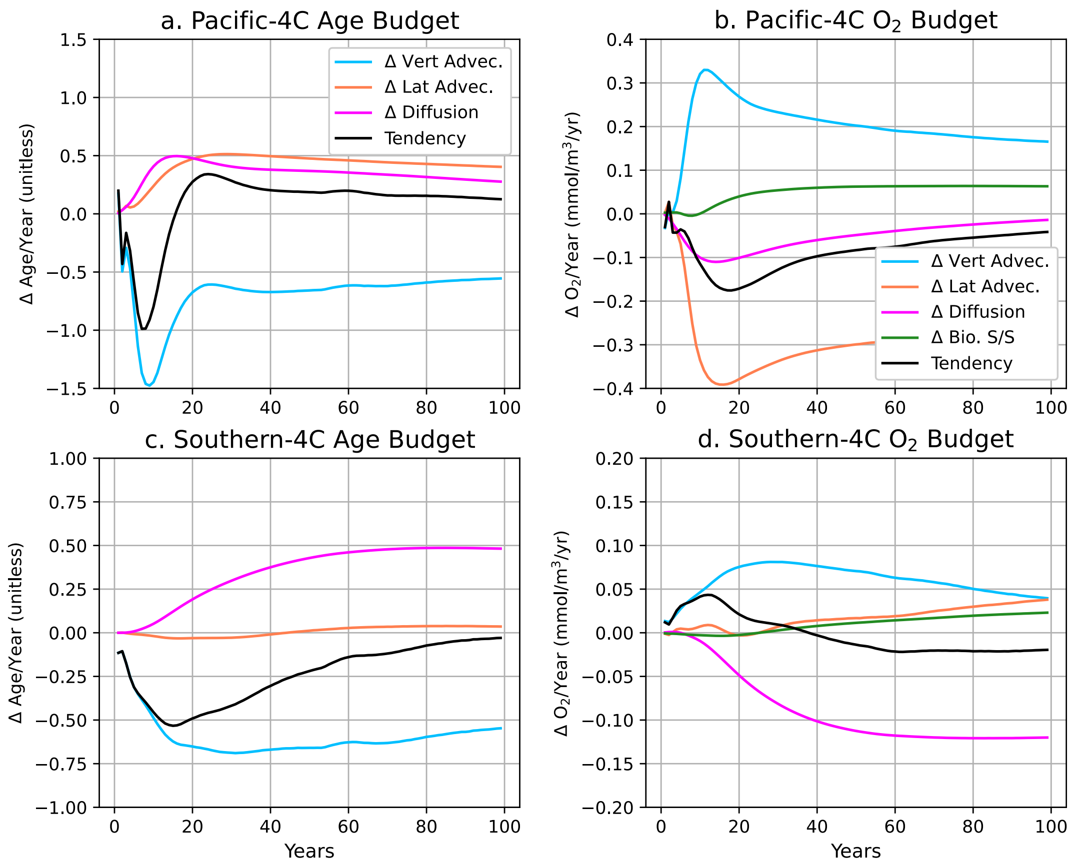

Figure 9. Evolution of Age and O_2 Budgets in the Eastern Tropical Pacific Thermocline. Budget terms are averaged over 195–985 m depth within the region of the eastern Tropical Pacific where the depth-averaged $O_2 < 100$ mmol/m^3 (within the "100" contour in Figure 4b). The differences between the budget terms for the perturbed and control runs are plotted. (a) Pacific-4C Age budget. (b) Pacific-4C O_2 budget. (c) Southern-4C Age budget. (d) Southern-4C O_2 budget.

solubility, whereas the surface boundary condition for age does not change. This surface anomaly is communicated to the OMZ by ventilation pathways, which are primarily lateral in the stratified tropical thermocline. Tropical O_2 loss is opposed by a decrease in respiration rate (Figures 6h and 9b). This is related to the simultaneous reduction of upwelling of nutrients into the euphotic zone, causing a suppression of productivity and export of organic matter to depth, similar to processes driving O_2 variability associated with climate modes (Deutsch et al., 2011). The impact of reduced respiration (OUR) on O_2 is less than half that of vertical advection change within our tropical OMZ region (Figure 9b), implying that biological changes are significant but not dominant.

4.3. Why Does Southern Ocean Warming Increase Ventilation of the Tropical and North Pacific?

The decrease in age under Global-4C across the tropics, eastern boundaries, and subpolar North Pacific is primarily driven by warming outside the Pacific basin, particularly in the Southern Ocean (Figure 4 and Figure S5 in Supporting Information S1). The Southern-4C experiment shows an age decrease and oxygenation of the whole North Pacific thermocline, but increased age across the South Pacific south of 10°S. We utilize a map (vertically averaged) view of age and O_2 budget terms, here averaged over the full 100-year run, to understand the geographic structure of the thermocline response. We show that this apparent hemispheric dipole is the result of two distinct dynamical responses: a fast downwelling Kelvin wave-driven response reduces age throughout the tropics and coastal regions, but advective and subsequent diffusive transport from the Southern Ocean gradually erodes the negative age anomaly in the South Pacific (Figures 9c, 9d, and 10).

The age and O_2 changes in the North Pacific (Figures 10a and 10b) are driven to first order by the change in vertical advection: weakened upwelling of old, low-O_2 waters leads to a decrease in age and increase in O_2

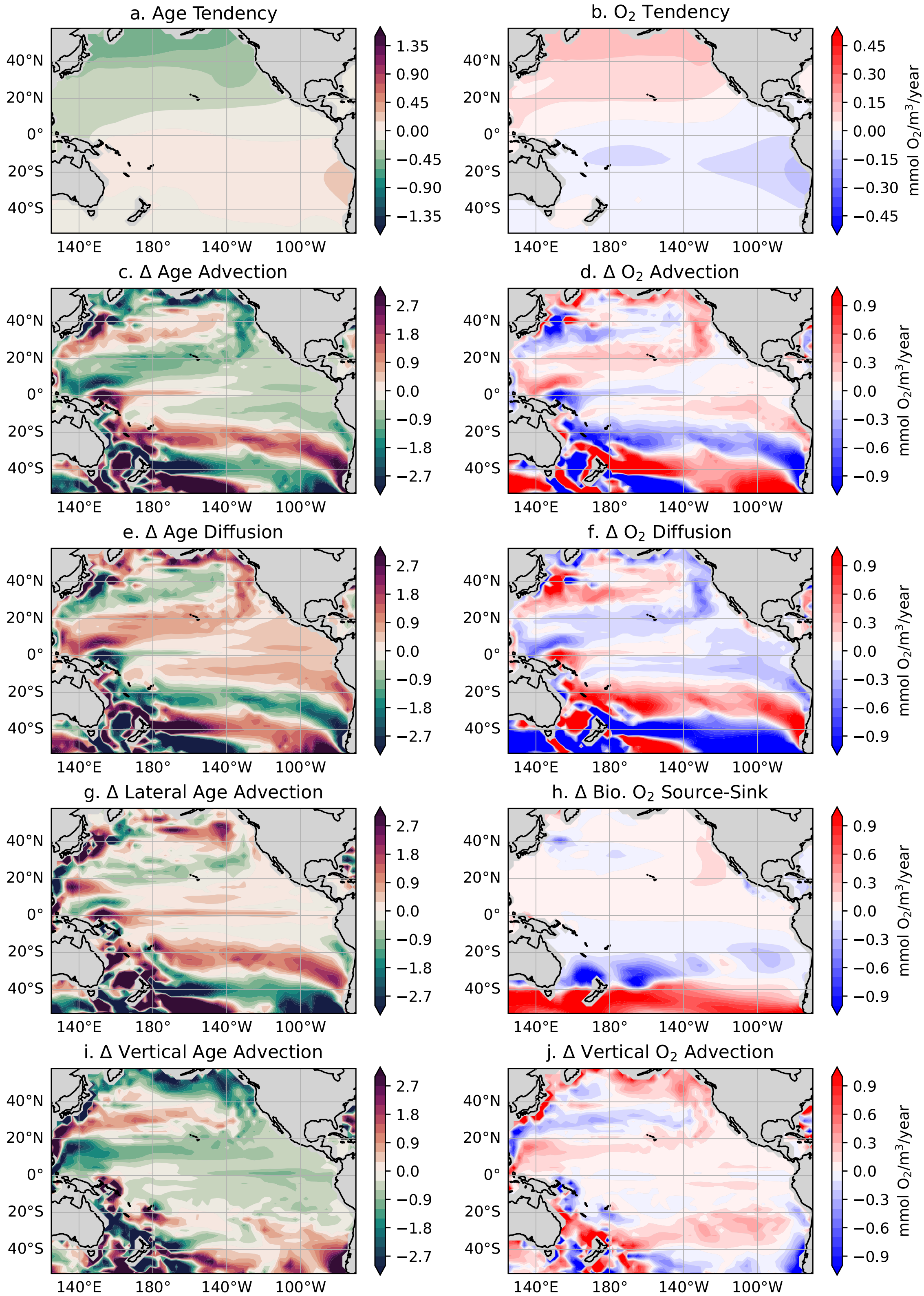

Figure 10. Age and O_2 budget maps for the Southern-4C experiment. These are averaged from 185 to 985 m in depth and over the full 100 years and differenced from the Control run. (a, b) Tendency of changing value, reflecting the total adjustment to warming (not the equilibrated values, as in Figure 6); note the compressed colorbar. (c, d) Total advective transport convergence changes. (e, f) Diffusive transport convergence changes. (g, i) Lateral and vertical components of advective age transport change, which sum to panel (c). (h) Changes in biological production and respiration of O_2. (j) Change in vertical transport of O_2.

(Figures 10i and 10j). This vertical advection anomaly is set by a dynamical adjustment of Pacific basin w to a warming-induced reduction in mode and intermediate water formation in the Southern Ocean (Figure 8b). Immediately following the SST step increase, reduced subduction (positive w') of suddenly warmer mode and intermediate water requires a compensating downward velocity change in an unstratified region outside the SST increase region, which in our model occurs near New Zealand. This downwelling anomaly spreads as a Kelvin wave (Movie S1): northward up the coast of Australia, eastward along the equator, then (having bifurcated at the coast of Ecuador) poleward along the North and South American coasts, from which it gradually propagates westward as a Rossby wave. Note that the vertical advection change is fairly hemispherically symmetric in the tropics (Figures 10i and 10j), as expected from a Kelvin wave. However, the North Pacific boundary wave produces a much stronger response than the South Pacific branch, because the South Pacific is damped by the Southern Ocean forcing. Vertical advection change dominates the age and O_2 changes in the eastern tropics in the first decade, because the wave-driven adjustment reaches this region faster than any physical transport from the Southern Ocean (Figures 9c and 9d).

In the South Pacific subtropical gyre, lateral advection change drives an age increase and O_2 loss (Figure 10g, also Figure 10d). Rather than a circulation change, this is related to the transport of anomalously older waters from the forced region (where ventilation is strongly reduced) by the mean gyre circulation, as evidenced by the slow northeastward progression in Movie S1. As the mode and intermediate water formation regions are lightened by the imposed forcing, the waters formed there now ventilate a shallower region of the South Pacific water column—leading to a sharp age increase in the subthermocline South Pacific that now outcrops much further south. The subtropical anomaly enters the tropical ocean primarily via along-isopycnal diffusion (via the parameterized eddy lateral mixing) across the southern subtropical-tropical boundary (Figures 9c, 9d, 10e, and 10f) and also via the low-latitude western boundary current and EUC (Figure 10g). This diffusive transport of anomalously higher age, lower O_2 water to the tropical OMZ takes much longer to reach its full strength under Southern-4C than under Pacific-4C (Figure 9), because the pathway from the Southern Ocean surface waters is longer; under NAtlantic-4C warming, the processes opposing vertical advection are very weak, as anomalously old water from the North Atlantic does not reach the tropical Pacific on these timescales (Figure S7 in Supporting Information S1). Similar to Pacific-4C, there is a weak biological O_2 gain in the tropics (Figures 9d and 10h) that reinforces advective O_2 increase, as reduced upwelling deprives the surface ocean of nutrients, decreasing productivity.

5. Summary and Discussion

In this study, we have explored the dynamics driving the spatial patterns of age and O_2 change in the Pacific basin under strong surface warming. While stratification increases and O_2 solubility decreases everywhere under global warming, subsurface ventilation shows a strong contrast: the North Pacific ventilated thermocline becomes older and significantly deoxygenated, while the tropical Pacific waters become more ventilated and experience little O_2 change. This "young get older, but old get younger" pattern in the tropical and subtropical North Pacific is consistently simulated across CMIP6 models under strong radiative forcing. We reproduce this contrasting pattern in a coarser ocean model forced by regionally distinct SST perturbations, with no wind stress change, and attribute it to a superposition of two distinct local and remote forcing effects and processes. First, local warming in the Pacific basin leads to a shoaling of the subtropical gyre, reducing the downwelling of young, oxygenated water in the subtropics. Second, remote forcing via warming in the Southern Ocean suppresses upwelling of old deep water in the tropical and eastern North Pacific via a wave-mediated dynamical adjustment (Figure 11).

While buoyancy addition in regions of subduction generally decreases ventilation rates (increases age) locally, we show here that the shoaling of subtropical gyre circulation under increased stratification concentrates this response at depth in the North Pacific subtropical gyre. This is a consequence of the dynamical adjustment of the subtropical circulation to intensified stratification: the vertical structure of the lateral flow is surface-intensified (Peng et al., 2022) and downwelling is strongly reduced within the subtropical thermocline. Subtropical surface water is still subducted and transported southward at rates dictated by the wind stress field (via Ekman pumping and Sverdrup balance), but in a warmer ocean, these ventilation pathways are confined to shallower depths, similar to the hypothesis of Oschlies et al. (2018). Our budget analysis of the warmed gyre shows that the distributions of the mean state processes have indeed shifted to shallower depths, resulting in a strong decrease of downward transport of O_2 and low-age water to the depths at the base of the previously ventilated thermocline. These depths are no longer reached by shoaling ventilation pathways along flattening isopycnals, leading to the

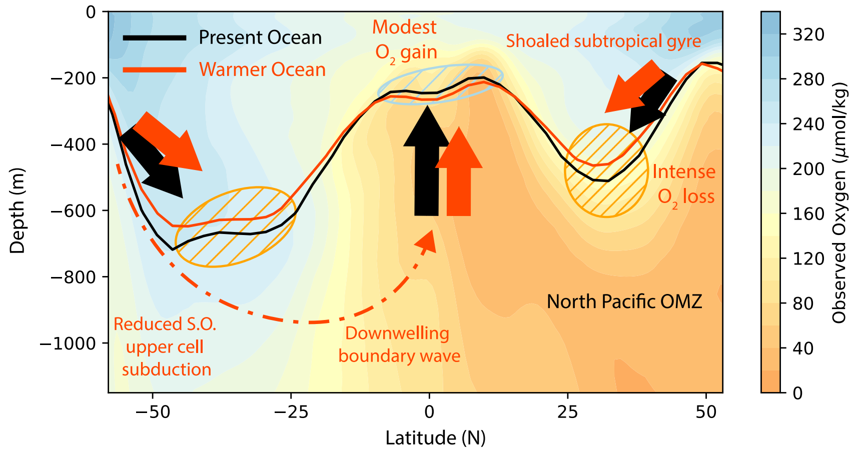

Figure 11. Schematic of the circulation and O_2 response to warming. The horizontal lines are contours of 150-year age in the Massachusetts Institute of Technology General Circulation Model Control and Global-4C experiments, reflecting the rapidly ventilated region. The background shading shows the WOA23 dissolved O_2 concentrations, averaged 180°W–135°W; the arrows and hatched ellipses illustrate circulation change and associated O_2 change, respectively.

sharp O_2 loss and age increase there. The shallower, flatter circulation also slows upwelling in the tropics, driving an opposite effect on O_2 and age there; thus uniform warming in the Pacific basin produces contrasting ventilation changes in the tropics and subtropics by slowing the background vertical circulation. Note the depth-integrated lateral volume transport changes little under warming, in contrast to its strong dependence on wind stress forcing (Duteil et al., 2014; McCreary & Lu, 1994); the same total transport is simply confined to a shallower layer. We thus suggest that the widespread O_2 loss projected at depth in the subtropical North Pacific in CMIP6 models (as documented in J. J. Busecke et al., 2022) is best explained by the shoaling of subtropical circulation, rather than a reduction in overall subtropical cell transport.

In contrast, the tropical Pacific shows significantly reduced upwelling under warmer SST forcing in the Pacific, Southern Ocean, and even North Atlantic. This slows the advection of old, low-O_2 waters into the tropical thermocline, driving a decrease in age and AOU as first reported by Gnanadesikan et al. (2007, 2012). Our experiments suggest that this decreased tropical upwelling results predominantly from an adjustment of ocean circulation to remote forcing from the Southern Ocean. The equatorial Pacific and eastern boundary regions are especially sensitive to these remote warming effects because they lie along the Kelvin waveguide which directs the basin-scale dynamical thermocline adjustment to applied warming (Sun et al., 2020); oxygenation along the eastern boundaries in these experiments appears primarily related to this downwelling wave, rather than the local surface densification emphasized by Gnanadesikan et al. (2012), as we have forced surface density to lighten everywhere. Reduced respiration (due to simultaneously suppressed surface production) also increases thermocline O_2, similarly to its modulation by climate variability via heave of the nutricline (Deutsch et al., 2011), but is less important than vertical advection in our simulations, consistent with J. J. Busecke et al. (2022). These tendencies toward tropical age decrease and oxygenation are opposed by the lateral advection and diffusion of anomalously under-ventilated waters from warmed water mass formation areas; thus, the regions further from these water mass formation areas are slower to experience deoxygenation and age increase.

5.1. Limitations of Model Experiments

Our MITgcm experiments have been conducted with an ocean model that is relatively coarse by modern standards and may not simulate well some key processes for ocean ventilation, especially in the tropical OMZ's. Our goal is not to simulate the magnitude of future O_2 change with high accuracy, but rather to illustrate to first order the dynamical drivers of a common response across CMIP models that our simpler model successfully reproduces. Still, our model exhibits notable biases in the climatological distribution of O_2; we consider here how these may impact our results. These mean state biases are generally similar to CMIP6 models' deficiencies (e.g., Cabré et al., 2015; Duteil et al., 2021), with excess O_2 in the shallow North Pacific OMZ and too little O_2 in the Southern Hemisphere intermediate waters, so that the simulated O_2 minimum is too deep in the water column. Biases in the vertical O_2 gradient influence the relative impact of vertical and lateral advection changes, especially at depths below the observed O_2 minimum. However, our essential mechanism holds within the strong North Pacific oxycline—between the well ventilated surface waters and the underlying O_2 minimum—despite imperfect representation of O_2 gradients in MITgcm: slower downwelling will reduce O_2 in the subtropics, and slower upwelling will increase O_2 in the tropical thermocline above the OMZ core.

When compared to a more realistic warming scenario, our experiments may overstate the impacts of Southern Ocean warming relative to Pacific warming. This is partially due to our experimental design: we apply a globally uniform SST change, whereas climate projections show relatively weak Southern Ocean warming due to buffering by background upwelling (Armour et al., 2016). Model bias may also play a role: MITgcm's mid-latitude Southern Ocean features unrealistically deep winter mixed layers (particularly around New Zealand, Figure S4 in Supporting Information S1) that are overly sensitive to surface warming (Sallée et al., 2013), whereas CMIP6 models represent these mixed layers more reasonably (Hong et al., 2021). Together with the absence of accelerating wind stress in our experiment, these factors amplify the ventilation decrease in MITgcm's Southern Pacific thermocline relative to CMIP6 (Figures 2c–2f). Additionally, the simplified coastal bathymetry in MITgcm favors the propagation of the Kelvin wave generated by Southern-4C (and other remote buoyancy forcing) far into the subpolar North Pacific (Figure 10j), which drives the strong age decrease and oxygenation of this region in both the Southern-4C and Global-4C experiments (Figures 4a, 4b, 4e, and 4f). Thus, discrepancies in the South Pacific and subpolar North Pacific between MITgcm warming experiments and the CMIP6 ensemble median may result from an overestimated role of Southern Ocean warming in our experiments, as well as the absence of wind stress or freshwater flux changes which can play key roles in these regions (Getzlaff et al., 2016; Hollitzer et al., 2024; Takano et al., 2018). Similar experiments conducted with higher resolution ocean models are needed to better constrain the sensitivity of Pacific basin O_2 to Southern Ocean warming. Future work should explore the important roles of westerly wind acceleration and freshwater addition in the Southern Pacific (e.g., Bronselaer et al., 2020), which might explain aspects of projected deoxygenation patterns not captured by our warming-only experiments.

5.2. Implications for Future Warming

While the dynamical adjustments to warming outlined here may already be at work in the observed ocean (e.g., Figure 1, Figure S1 in Supporting Information S1), the observational record of dissolved O_2 is impacted by sparse sampling (Ito et al., 2026), higher-frequency wind stress changes (Hollitzer et al., 2024), and non-uniform warming, making the O_2 trends driven by broad warming difficult to isolate (e.g., Long et al., 2016). In the North Pacific, the Pacific Decadal Oscillation drives strong natural variability that obscures anthropogenic trends (Duteil et al., 2018; Stramma et al., 2020); moreover, aerosol deposition (Ito et al., 2016) may amplify the GHG-driven warming effects on O_2 via enhanced deposition of micronutrients, increased production, and intensified O_2 consumption at depth. Like the Pacific, the Atlantic basin shows stronger deoxygenation in the subtropics than the tropics in future projections (Kwiatkowski et al., 2020). Similar warming-driven circulation changes such as slowing vertical velocities likely contribute to this contrast (Gnanadesikan et al., 2007), with tropical Atlantic upwelling potentially repressed by reduced North Atlantic Deep Water formation and AMOC slowdown. Still, North Pacific O_2 concentrations are uniquely sensitive to vertical circulation change because of the basin's sharp oxycline (Figure 11), the result of the limited extent of North Pacific Intermediate Water (Talley, 1993) and absence of deep water formation in the North Pacific. Thus, deoxygenation at the base of the North Pacific ventilated thermocline (Figures 1f, Kwon et al., 2016; Mecking et al., 2008) could plausibly be the emergence of an anthropogenic signal, but reducing uncertainty and parsing other variability remains challenging. Ongoing analysis of the inconsistencies in O_2 change between and among observational estimates and climate models (e.g., Gridded Observational Data set Intercomparison Project-Dissolved Oxygen (GODIP-DO) and Integration of Models and Observations across Scales (INMOS)) (Du et al., 2026) will lay the groundwork for a more certain determination (Ito et al., 2026), provided that global thermocline oxygen observations continue to be made available by the Biogeochemical-Argo program (Chamberlain et al., 2023).

Whether through reduced deep water formation in the high latitudes or the shoaled vertical structure in the subtropics, increased stratification tends to reduce vertical velocities—perhaps because vertical movements require more potential energy. This generality provides a unifying explanation for the "young get older, but old get younger" pattern: thermocline waters kept young by climatological downwelling become older as the downwelling slows at mid-latitudes, whereas thermocline waters kept old by upwelled deep water become younger as upwelling is reduced. Provided that this modeled mechanism operates with similar strength in the future ocean, this is welcome news for poorly ventilated OMZ's threatened by increased temperatures. It suggests that future deoxygenation in the OMZ's should be relatively modest over the coming century, even without a slackening of the trade winds - though low-O_2 environments are sensitive to even small changes. On the other hand, oxygen loss deep in the North Pacific thermocline, in conjunction with increasing temperatures, will compress the metabolically tolerable habitat for a wide range of species (Deutsch et al., 2020; Fröb et al., 2024; Mongwe et al., 2024). These warming-induced circulation changes play a key role in shaping the Pacific Ocean's physical, biogeochemical and ecosystem response to anthropogenic climate change.

Conflict of Interest

The authors declare no conflicts of interest relevant to this study.

Availability Statement

MITgcm (Checkpoint 68c, https://github.com/MITgcm/MITgcm/) was used in all our model experiments. Model output and configuration files are stored at https://doi.org/10.5281/zenodo.20329786 (Taylor, 2026), and analysis code to reproduce figures is stored at https://doi.org/10.5281/zenodo.20279261. Processed CMIP6 data sets are available at https://zenodo.org/records/6799334 (J. Busecke, 2022). Hydrographic data is available from https://cchdo.ucsd.edu/. Argo mixed layer depth is available at https://mixedlayer.ucsd.edu/.

Acknowledgments

B.A.T. and L.D.T. were supported by NSF's Southern Ocean Carbon and Climate Observations and Modeling (SOCCOM) project (OPP-1936222). Y.A.E. acknowledges support from NSF OCE-1948599, OCE-2421546, and NOAA NA24OARX431C0018. Y.T. was supported by a joint UK Natural Environment Research Council and (US) NSF Large Grant NE/W009501/1 (C-Streams). We acknowledge high-performance computing support from the Derecho system (https://doi.org/10.5065/qx9a-pg09) provided by the NSF National Center for Atmospheric Research (NCAR) under NSF OCE-2421546 project support. We thank the scientists and crews involved in collecting and making available O_2 measurements presented here, and T. Ito and collaborators for their gridded O_2 data set. We also thank the modeling centers that created and made available the CMIP6 data used here, and J. Busecke and collaborators for consolidating these data sets. We acknowledge helpful discussion with S. Sun and helpful feedback from two anonymous reviewers. Prov 3:6.

References

Abernathey, R., Busecke, J., Smith, T., Banihirwe, A., Bot, S., Bourbeau, J., et al. (2020). xgcm/xgcm: V0.5.2. *Zenodo*. https://doi.org/10.5281/zenodo.4097223

Armour, K. C., Marshall, J., Scott, J. R., Donohoe, A., & Newsom, E. R. (2016). Southern ocean warming delayed by circumpolar upwelling and equatorward transport. *Nature Geoscience*, *9*(7), 549–554.

Bettencourt, J. H., López, C., Hernández-García, E., Montes, I., Sudre, J., Dewitte, B., et al. (2015). Boundaries of the peruvian oxygen minimum zone shaped by coherent mesoscale dynamics. *Nature Geoscience*, *8*(12), 937.

Bopp, L., Resplandy, L., Untersee, A., Le Mezo, P., & Kageyama, M. (2017). Ocean (de) oxygenation from the last glacial maximum to the twenty-first century: Insights from earth system models. *Philosophical Transactions of the Royal Society A: Mathematical, Physical and Engineering Sciences*, *375*(2102), 20160323. https://doi.org/10.1098/rsta.2016.0323

Bronselaer, B., Russell, J. L., Winton, M., Williams, N. L., Key, R. M., Dunne, J. P., et al. (2020). Importance of wind and meltwater for observed chemical and physical changes in the southern ocean. *Nature Geoscience*, *13*(1), 35–42.

Bryan, K., & Lewis, L. (1979). A water mass model of the world ocean. *Journal of Geophysical Research*, *84*(C5), 2503–2517.

Busecke, J. (2022). Data for "Diverging fates of the Pacific Ocean oxygen minimum zone and its core in a warming world" (2022, AGU Advances) [Dataset]. *Zenodo*. https://doi.org/10.5281/zenodo.6799334

Busecke, J. J., Resplandy, L., Ditkovsky, S. J., & John, J. G. (2022). Diverging fates of the Pacific Ocean oxygen minimum zone and its core in a warming world. *AGU Advances*, *3*(6), e2021AV000470. https://doi.org/10.1029/2021AV000470

Cabré, A., Marinov, I., Bernardello, R., & Bianchi, D. (2015). Oxygen minimum zones in the tropical pacific across CMIP5 models: Mean state differences and climate change trends. *Biogeosciences*, *12*(18), 5429–5454.

Chamberlain, P., Talley, L. D., Cornuelle, B., Mazloff, M., & Gille, S. T. (2023). Optimizing the biogeochemical Argo float distribution. *Journal of Atmospheric and Oceanic Technology*, *40*(11), 1355–1379.

Couespel, D., Davila, X., Goris, N., Jeansson, E., Lauvset, S. K., & Tjiputra, J. (2026). Divergent sensitivities of apparent oxygen utilization to ventilation changes in the deep ocean across Earth system models. *Biogeosciences*, *23*(10), 3433–3466. https://doi.org/10.5194/bg-23-3433-2026

Couespel, D., Lévy, M., & Bopp, L. (2019). Major contribution of reduced upper ocean oxygen mixing to global ocean deoxygenation in an earth system model. *Geophysical Research Letters*, *46*(21), 12239–12249. https://doi.org/10.1029/2019GL084162

Deutsch, C., Berelson, W., Thunell, R., Weber, T., Tems, C., McManus, J., et al. (2014). Centennial changes in north Pacific anoxia linked to tropical trade winds. *Science*, *345*(6197), 665–668.

Deutsch, C., Brix, H., Ito, T., Frenzel, H., & Thompson, L. (2011). Climate-forced variability of ocean hypoxia. *Science*, *333*(6040), 336–339.

Deutsch, C., Penn, J. L., & Seibel, B. (2020). Metabolic trait diversity shapes marine biogeography. *Nature*, *585*(7826), 557–562.

Ditkovsky, S., & Resplandy, L. (2025). Unifying future ocean oxygen projections using an oxygen water mass framework. *Journal of Geophysical Research: Oceans*, *130*(5), e2025JC022333. https://doi.org/10.1029/2025JC022333

Du, J., Cheng, L., Ito, T., Garcia, H. E., Wang, Z., Sharp, J. D., et al. (2026). Climatology and annual cycle of global ocean dissolved oxygen represented by multiple observational gridded products. *Ocean Science*, *22*(3), 1483–1499.

Duteil, O., Böning, C. W., & Oschlies, A. (2014). Variability in subtropical-tropical cells drives oxygen levels in the tropical Pacific Ocean. *Geophysical Research Letters*, *41*(24), 8926–8934. https://doi.org/10.1002/2014GL061774

Duteil, O., Frenger, I., & Getzlaff, J. (2021). The riddle of eastern tropical Pacific Ocean oxygen levels: The role of the supply by intermediate-depth waters. *Ocean Science*, *17*(5), 1489–1507.

Duteil, O., Oschlies, A., & Böning, C. W. (2018). Pacific decadal oscillation and recent oxygen decline in the eastern tropical Pacific Ocean. *Biogeosciences*, *15*(23), 7111–7126.

Dutkiewicz, S., Sokolov, A. P., Scott, J., & Stone, P. H. (2005). A three-dimensional ocean-sea ice-carbon cycle model and its coupling to a two-dimensional atmospheric model: Uses in climate change studies (Technical Report). In *MIT Joint Program on the science and Policy of global change*.

Eddebbar, Y. A., Whitt, D. B., Verdy, A., Mazloff, M. R., Subramanian, A. C., & Long, M. C. (2024). Eddy-mediated turbulent mixing of oxygen in the equatorial pacific. *Journal of Geophysical Research: Oceans*, *129*(3), e2023JC020588. https://doi.org/10.1029/2023JC020588

Emerson, S., Watanabe, Y. W., Ono, T., & Mecking, S. (2004). Temporal trends in apparent oxygen utilization in the upper pycnocline of the north pacific: 1980–2000. *Journal of Oceanography*, *60*(1), 139–147.

Feely, R. A., Sabine, C. L., Schlitzer, R., Bullister, J. L., Mecking, S., & Greeley, D. (2004). Oxygen utilization and organic carbon remineralization in the upper water column of the Pacific Ocean. *Journal of Oceanography*, *60*(1), 45–52.

Fröb, F., Bourgeois, T., Goris, N., Schwinger, J., & Heinze, C. (2024). Simulated abrupt shifts in aerobic habitats of marine species in the past, present, and future. *Earth's Future*, *12*(4), e2023EF004141.

Garcia, H., Wang, Z., Bouchard, C., Cross, S., Paver, C., Reagan, J., et al. (2024). *World ocean atlas 2023. Volume 3: Dissolved oxygen, apparent oxygen utilization, dissolved oxygen saturation, and 30-year climate normal (Technical Report)*. NOAA Atlas NESDIS. https://doi.org/10.25923/rb67-ns53

Garcia, H. E., Weathers, K., Paver, C. R., Smolyar, I., Boyer, T. P., Locarnini, R. A., et al. (2019). *World ocean atlas 2018, volume 3: Dissolved oxygen, apparent oxygen utilization, and oxygen saturation (Technical Report)*. NOAA Atlas NESDIS. https://doi.org/10.25923/qspr-pn52

Gent, P. R., & Mcwilliams, J. C. (1990). Isopycnal mixing in ocean circulation models. *Journal of Physical Oceanography*, *20*(1), 150–155.

Getzlaff, J., Dietze, H., & Oschlies, A. (2016). Simulated effects of southern hemispheric wind changes on the pacific oxygen minimum zone. *Geophysical Research Letters*, *43*(2), 728–734. https://doi.org/10.1002/2015GL066841

Gnanadesikan, A., Dunne, J., & John, J. (2012). Understanding why the volume of suboxic waters does not increase over centuries of global warming in an earth system model. *Biogeosciences*, *9*(3), 1159–1172.

Gnanadesikan, A., Russell, J., & Russell, J. (2007). How does ocean ventilation change under global warming? *Ocean Science*, *3*(1), 43–53. https://doi.org/10.5194/os-3-43-2007

Hollitzer, H. A., Patara, L., Terhaar, J., & Oschlies, A. (2024). Competing effects of wind and buoyancy forcing on ocean oxygen trends in recent decades. *Nature Communications*, *15*(1), 9264. https://doi.org/10.1038/s41467-024-53557-y

Hong, Y., Du, Y., Xia, X., Xu, L., Zhang, Y., & Xie, S.-P. (2021). Subantarctic mode water and its long-term change in CMIP6 models. *Journal of Climate*, *34*(23), 9385–9400.

Ito, T. (2022). *Optimal interpolation of global dissolved oxygen: 1965–2015*. Wiley Online Library. https://doi.org/10.26008/1912/bco-dmo.816978.2

Ito, T., Cervania, A., Cross, K., Ainchwar, S., & Delawalla, S. (2024). Mapping dissolved oxygen concentrations by combining shipboard and Argo observations using machine learning algorithms. *Journal of Geophysical Research: Machine Learning and Computation*, *1*(3), e2024JH000272.

Ito, T., Long, M. C., Deutsch, C., Minobe, S., & Sun, D. (2019). Mechanisms of low-frequency oxygen variability in the north pacific. *Global Biogeochemical Cycles*, *33*(2), 110–124. https://doi.org/10.1029/2018GB005987

Ito, T., Nenes, A., Johnson, M., Meskhidze, N., & Deutsch, C. (2016). Acceleration of oxygen decline in the tropical pacific over the past decades by aerosol pollutants. *Nature Geoscience*, *9*(6), 443–447. https://doi.org/10.1038/ngeo2717

Ito, T., Takano, Y., Deutsch, C., & Long, M. C. (2022). Sensitivity of global ocean deoxygenation to vertical and isopycnal mixing in an ocean biogeochemistry model. *Global Biogeochemical Cycles*, *36*(4), e2021GB007151. https://doi.org/10.1029/2021GB007151

Ito, T., Takano, Y., Eddebbar, Y. A., Tiputra, J. F., Wang, Z., Minobe, S., et al. (2026). Are simulated Ocean deoxygenation rates consistent with the observational reconstructions? *Annual Review of Earth and Planetary Sciences*, *54*. https://doi.org/10.1146/annurev-earth-032524-123111

Jenkins, W. (1982). Oxygen utilization rates in North Atlantic subtropical gyre and primary production in oligotrophic systems. *Nature*, *300*(5889), 246–248.

Jiang, S., Stone, P. H., & Malanotte-Rizzoli, P. (1999). An assessment of the Geophysical Fluid Dynamics Laboratory ocean model with coarse resolution: Annual-mean climatology. *Journal of Geophysical Research*, *104*(C11), 25623–25645.

Karstensen, J., Stramma, L., & Visbeck, M. (2008). Oxygen minimum zones in the eastern tropical Atlantic and Pacific Oceans. *Progress in Oceanography*, *77*(4), 331–350.

Keeling, R. F., Körtzinger, A., & Gruber, N. (2010). Ocean deoxygenation in a warming world. *Annual Review of Marine Science*, *2*(1), 199–229.

Kuhn, A. M., Mazloff, M. R., Gille, S. T., & Verdy, A. (2025). Sensitivity of chlorophyll vertical structure to model parameters in the biogeochemical southern ocean state estimate (B-SOSE). *Journal of Geophysical Research: Biogeosciences*, *130*(1), e2024JG008300. https://doi.org/10.1029/2024JG008300

Kwiatkowski, L., Torres, O., Bopp, L., Aumont, O., Chamberlain, M., Christian, J. R., et al. (2020). Twenty-first century ocean warming, acidification, deoxygenation, and upper-ocean nutrient and primary production decline from CMIP6 model projections. *Biogeosciences*, *17*(13), 3439–3470.

Kwon, E. Y., Deutsch, C., Xie, S.-P., Schmidtko, S., & Cho, Y.-K. (2016). The north pacific oxygen uptake rates over the past half century. *Journal of Climate*, *29*(1), 61–76.

Lam, P., Lavik, G., Jensen, M. M., van de Vossenberg, J., Schmid, M., Woebken, D., et al. (2009). Revising the nitrogen cycle in the Peruvian oxygen minimum zone. *Proceedings of the National Academy of Sciences*, *106*(12), 4752–4757. https://doi.org/10.1073/pnas.0812444106

Levitus, S., Burgett, R., & Boyer, T. P. (1994). *World ocean atlas 1994, salinity (Technical Report)* (Vol. 3). NOAA Atlas NESDIS.

Lévy, M., Resplandy, L., Palter, J. B., Couespel, D., & Lachkar, Z. (2022). The crucial contribution of mixing to present and future ocean oxygen distribution. In *Ocean mixing* (pp. 329–344). Elsevier.

Liu, C., & Wang, Z. (2014). On the response of the global subduction rate to globalwarming in coupled climate models. *Advances in Atmospheric Sciences*, *31*(1), 211–218. https://doi.org/10.1007/s00376-016-6021-2

Llanillo, P., Pelegrí, J. L., Talley, L., Peña-Izquierdo, J., & Cordero, R. R. (2018). Oxygen pathways and budget for the eastern south pacific oxygen minimum zone. *Journal of Geophysical Research: Oceans*, *123*(3), 1722–1744. https://doi.org/10.1002/2017JC013509

Long, M. C., Deutsch, C., & Ito, T. (2016). Finding forced trends in oceanic oxygen. *Global Biogeochemical Cycles*, *30*(2), 381–397. https://doi.org/10.1002/2015GB005310

Luongo, M. T., Xie, S.-P., Eisenman, I., Sun, S., & Peng, Q. (2025). How the subsurface tropical pacific responds to subtropical surface cooling: Implications for cross-equatorial transport. *Journal of Climate*. https://doi.org/10.1175/JCLI-D-24-0440.1

Luyten, J., Pedlosky, J., & Stommel, H. (1983). The ventilated thermocline. *Journal of Physical Oceanography*, *13*(2), 292–309.

Margolskee, A., Frenzel, H., Emerson, S., & Deutsch, C. (2019). Ventilation pathways for the north pacific oxygen deficient zone. *Global Biogeochemical Cycles*, *33*(7), 875–890. https://doi.org/10.1029/2018GB006149

Marshall, J., Adcroft, A., Hill, C., Perelman, L., & Heisey, C. (1997). A finite-volume, incompressible Navier stokes model for studies of the ocean on parallel computers. *Journal of Geophysical Research*, *102*(C3), 5753–5766.

Marshall, J., Hill, C., Perelman, L., & Adcroft, A. (1997). Hydrostatic, quasi-hydrostatic, and nonhydrostatic ocean modeling. *Journal of Geophysical Research*, *102*(C3), 5733–5752.

McCreary, J. P., Jr., & Lu, P. (1994). Interaction between the subtropical and equatorial ocean circulations: The subtropical cell. *Journal of Physical Oceanography*, *24*(2), 466–497.

Mecking, S., & Drushka, K. (2024). Linking northeastern North Pacific oxygen changes to upstream surface outcrop variations. *Biogeosciences*, *21*(5), 1117–1133. https://doi.org/10.1029/2007GB003101

Mecking, S., Langdon, C., Feely, R. A., Sabine, C. L., Deutsch, C. A., & Min, D.-H. (2008). Climate variability in the North Pacific thermocline diagnosed from oxygen measurements: An update based on the US CLIVAR/CO2 Repeat Hydrography cruises. *Global Biogeochemical Cycles*, *22*(3), GB3015. https://doi.org/10.1029/2007GB003101

Mongwe, P., Long, M., Ito, T., Deutsch, C., & Santana-Falcón, Y. (2024). Climatic controls on metabolic constraints in the ocean. *Biogeosciences*, *21*(15), 3477–3490.

Newsom, E., Zanna, L., & Khatiwala, S. (2022). Relating patterns of added and redistributed ocean warming. *Journal of Climate*, *35*(14), 4627–4643.

Oschlies, A., Brandt, P., Stramma, L., & Schmidtko, S. (2018). Drivers and mechanisms of ocean deoxygenation. *Nature Geoscience*, *11*(7), 467–473.

Parekh, P., Follows, M. J., & Boyle, E. A. (2005). Decoupling of iron and phosphate in the global ocean. *Global Biogeochemical Cycles*, *19*(2). https://doi.org/10.1029/2004GB002280

Peng, Q., Xie, S.-P., Wang, D., Huang, R. X., Chen, G., Shu, Y., et al. (2022). Surface warming–induced global acceleration of upper ocean currents. *Science Advances*, *8*(16), eabj8394. https://doi.org/10.1126/sciadv.abj8394

Portela, E., Kolodziejczyk, N., Vic, C., & Thierry, V. (2020). Physical mechanisms driving oxygen subduction in the global ocean. *Geophysical Research Letters*, *47*(17), e2020GL089040. https://doi.org/10.1029/2020GL089040

Poupon, M. A., Resplandy, L., Lévy, M., & Bopp, L. (2023). Pacific Decadal Oscillation influences tropical oxygen minimum zone extent and obscures anthropogenic changes. *Geophysical Research Letters*, *50*(7), e2022GL102123. https://doi.org/10.1029/2022GL102123

Redi, M. H. (1982). Oceanic isopycnal mixing by coordinate rotation. *Journal of Physical Oceanography*, *12*(10), 1154–1158.

Roach, C. J., & Bindoff, N. L. (2023). Developing a new oxygen atlas of the world's oceans using data interpolating variational analysis. *Journal of Atmospheric and Oceanic Technology*, *40*(11), 1475–1491.

Sallée, J.-B., Shuckburgh, E., Bruneau, N., Meijers, A. J., Bracegirdle, T. J., & Wang, Z. (2013). Assessment of southern ocean mixed-layer depths in CMIP5 models: Historical bias and forcing response. *Journal of Geophysical Research: Oceans*, *118*(4), 1845–1862. https://doi.org/10.1002/jgrc.20157

Stramma, L., Schmidtko, S., Bograd, S. J., Ono, T., Ross, T., Sasano, D., & Whitney, F. A. (2020). Trends and decadal oscillations of oxygen and nutrients at 50 to 300 m depth in the equatorial and north pacific. *Biogeosciences*, *17*(3), 813–831.

Sulpis, O., Trossman, D. S., Holzer, M., Jeansson, E., Lauvset, S. K., & Middelburg, J. J. (2023). Respiration patterns in the dark ocean. *Global Biogeochemical Cycles*, *37*(8), e2023GB007747. https://doi.org/10.1029/2023GB007747

Sun, S., Thompson, A. F., & Eisenman, I. (2020). Transient overturning compensation between Atlantic and indo-Pacific basins. *Journal of Physical Oceanography*, *50*(8), 2151–2172.

Sun, S., Thompson, A. F., Xie, S.-P., & Long, S.-M. (2022). Indo-pacific warming induced by a weakening of the Atlantic meridional overturning circulation. *Journal of Climate*, *35*(2), 815–832. https://doi.org/10.1175/JCLI-D-21-0346.1

Sverdrup, H. (1938). On the explanation of the oxygen minima and maxima in the oceans. *ICES Journal of Marine Science*, *13*(2), 163–172.

Takano, Y., Ilyina, T., Tjiputra, J., Eddebbar, Y. A., Berthet, S., Bopp, L., et al. (2023). Simulations of ocean deoxygenation in the historical era: Insights from forced and coupled models. *Frontiers in Marine Science*, *10*, 1139917.

Takano, Y., Ito, T., & Deutsch, C. (2018). Projected centennial oxygen trends and their attribution to distinct ocean climate forcings. *Global Biogeochemical Cycles*, *32*(9), 1329–1349. https://doi.org/10.1029/2018GB005939

Talley, L. D. (1988). Potential vorticity distribution in the north pacific. *Journal of Physical Oceanography*, *18*(1), 89–106.

Talley, L. D. (1993). Distribution and formation of North Pacific intermediate water. *Journal of Physical Oceanography*, *23*(3), 517–537.

Taylor, B. A. (2026). Data for: "young get older, but old get younger": Warming-induced circulation change explains contrasting pattern of projected Pacific deoxygenation [Dataset]. *Zenodo*. https://doi.org/10.5281/zenodo.20329786

Taylor, B. A., Shi, J.-R., Xie, S.-P., Talley, L. D., Luongo, M. T., & Peng, Q. (2025). Warming band in southern ocean's Indian sector: The role of remote Atlantic buoyancy forcing via poleward-shifting circulation response. *Journal of Climate*, *38*(14), 3219–3238.

Trenberth, K. E., Large, W. G., & Olson, J. G. (1990). The mean annual cycle in global ocean wind stress. *Journal of Physical Oceanography*, *20*(11), 1742–1760.

Wang, G., Xie, S.-P., Huang, R. X., & Chen, C. (2015). Robust warming pattern of global subtropical oceans and its mechanism. *Journal of Climate*, *28*(21), 8574–8584.

Wyrtki, K. (1962). The oxygen minima in relation to ocean circulation. *Deep Sea Research and Oceanographic Abstracts*, *9*(1), 11–23. https://doi.org/10.1016/0011-7471(62)90243-7

Zhang, B., Linz, M., Sun, S., & Thompson, A. F. (2024). A framework for constraining ocean mixing rates and overturning circulation from age tracers. *Journal of Physical Oceanography*, *54*(8), 1583–1602.

References From the Supporting Information

Bentsen, M., Oliviè, D. J. L., Seland, Ø., Toniazzo, T., Gjermundsen, A., Graff, L. S., et al. (2019). *NCC NorESM2-MM model output prepared for CMIP6 CMIP*. World Data Center for Climate (WDCC) at DKRZ.

Boucher, O., Servonnat, J., Albright, A. L., Aumont, O., Balkanski, Y., Bastrikov, V., et al. (2020). Presentation and evaluation of the IPSL-CM6A-LR climate model. *Journal of Advances in Modeling Earth Systems*, *12*(7), e2019MS002010. https://doi.org/10.1029/2019MS002010

Christian, J. R., Denman, K. L., Hayashida, H., Holdsworth, A. M., Lee, W. G., Riche, O. G., et al. (2021). Ocean biogeochemistry in the Canadian earth system model version 5.0.3: CanESM5 and CanESM5-CanOE. In *Geoscientific Model Development Discussions (GMDD), 2021* (pp. 1–68).

Guo, H., John, J. G., Blanton, C., McHugh, C., Nikonov, S., Radhakrishnan, A., et al. (2018). *NOAA-GFDL GFDL-CM4 model output prepared for CMIP6 ScenarioMIP SSP585*. Earth System Grid Federation.

Hajima, T., Watanabe, M., Yamamoto, A., Tatebe, H., Noguchi, M. A., Abe, M., et al. (2020). Development of the MIROC-ES2L Earth system model and the evaluation of biogeochemical processes and feedbacks. *Geoscientific Model Development*, *13*(5), 2197–2244. https://doi.org/10.5194/gmd-13-2197-2020

Holte, J., Talley, L. D., Gilson, J., & Roemmich, D. (2017). An Argo mixed layer climatology and database. *Geophysical Research Letters*, *44*(11), 5618–5626. https://doi.org/10.1002/2017GL073426

Jungclaus, J., Bittner, M., Wieners, K.-H., Wachsmann, F., Schupfner, M., Legutke, S., et al. (2019). *MPI-M MPI ESM1.2-HR model output prepared for CMIP6 CMIP*. Earth System Grid Federation. https://doi.org/10.22033/ESGF/CMIP6.741

Krasting, J. P., John, J. G., Blanton, C., McHugh, C., Nikonov, S., Radhakrishnan, A., et al. (2018). *NOAA-GFDL GFDL-ESM4 model output prepared for CMIP6*. World Data Center for Climate (WDCC) at DKRZ.

Séférian, R., Nabat, P., Michou, M., Saint-Martin, D., Voldoire, A., Colin, J., et al. (2019). Evaluation of CNRM Earth system model, CNRM-ESM2-1: Role of Earth system processes in present-day and future climate. *Journal of Advances in Modeling Earth Systems*, *11*(12), 4182–4227. https://doi.org/10.1029/2019MS001791

Seland, Ø., Bentsen, M., Olivié, D. J. L., Toniazzo, T., Gjermundsen, A., Graff, L. S., et al. (2019). *NCC NorESM2-LM model output prepared for CMIP6 CMIP historical*. World Data Center for Climate (WDCC) at DKRZ.

Swart, N. C., Cole, J. N., Kharin, V. V., Lazare, M., Scinocca, J. F., Gillett, N. P., et al. (2019). The Canadian earth system model version 5 (CanESM5.0.3). *Geoscientific Model Development*, *12*(11), 4823–4873.

Tang, Y., Rumbold, S., Ellis, R., Kelley, D., Mulcahy, J., Sellar, A., et al. (2019). *MOHC UKESM1.0-LL model output prepared for CMIP6 CMIP*. Earth System Grid Federation. https://doi.org/10.22033/ESGF/CMIP6.1569

Wieners, K.-H., Giorgetta, M., Jungclaus, J., Reick, C., Esch, M., Bittner, M., et al. (2019). *MPI-M MPIESM1.2-LR model output prepared for CMIP6 CMIP*. Earth System Grid Federation. https://doi.org/10.22033/ESGF/CMIP6.742

Yukimoto, S., Kawai, H., Koshiro, T., Oshima, N., Yoshida, K., Urakawa, S., et al. (2019). The Meteorological Research Institute Earth System Model version 2.0, MRI-ESM2.0: Description and basic evaluation of the physical component. *Journal of the Meteorological Society of Japanese Series II*, *97*(5), 931–965.

Ziehn, T., Chamberlain, M. A., Law, R. M., Lenton, A., Bodman, R. W., Dix, M., et al. (2020). The Australian earth system model: ACCESS-ESM1.5. *Journal of Southern Hemisphere Earth Systems Science*, *70*(1), 193–214. https://doi.org/10.1071/ES19035